The Astronomical Journal, 150:24 (21pp), 2015 July doi:10.1088/0004-6256/150/1/24

KINEMATICS AND STELLAR POPULATIONS IN ISOLATED LENTICULAR GALAXIES*

Ivan Yu. Katkov[1], Alexei Yu. Kniazev[1,2,3], and Olga K. Sil'chenko[1,4]
[1] Sternberg Astronomical Institute, M.V. Lomonosov Moscow State University, Universitetsky pr., 13, Moscow, 119991 Russia; katkov@sai.msu.ru, olga@sai.msu.su
[2] South African Astronomical Observatory, P.O. Box 9, 7935 Observatory, Cape Town, South Africa; akniazev@saao.ac.za
[3] Southern African Large Telescope Foundation, P.O. Box 9, 7935 Observatory, Cape Town, South Africa
[4] Isaac Newton Institute, Moscow Branch, Chile
Received 2014 October 28; accepted 2015 April 29; published 2015 July 1

ABSTRACT

By combining new long-slit spectral data obtained with the Southern African Large Telescope for nine galaxies with our previously published observations for 12 additional galaxies, we study the stellar and gaseous kinematics as well as radially resolved stellar population properties and ionized-gas metallicity and excitation for a sample of isolated lenticular galaxies. We have found that there is no particular time frame of formation for the isolated lenticular galaxies: the mean stellar ages of the bulges and disks are distributed between 1 and >13 Gyr, and the bulge and the disk in every galaxy formed synchronously demonstrate similar stellar ages and magnesium-to-iron ratios. Extended ionized-gas disks are found in the majority of the isolated lenticular galaxies, in 72% ±11%. Half of all extended gaseous disks demonstrate a visible counterrotation with respect to their stellar counterparts. We argue that just such a fraction of projected counterrotation is expected if all of the gas in isolated lenticular galaxies is accreted from outside, under the assumption of isotropically distributed external sources. The very narrow range of the gas oxygen abundances we found for the outer ionized-gas disks excited by young stars, [O/H] from 0.0 to +0.2 dex, gives evidence for satellite merging as the most probable source of this accretion. Last, we formulate a hypothesis that the morphological type of a field disk galaxy is completely determined by the outer cold-gas accretion regime.

Key words: galaxies: elliptical and lenticular, cD – galaxies: evolution – galaxies: formation – galaxies: kinematics and dynamics – galaxies: structure

1. INTRODUCTION

Understanding the processes of galaxy formation and evolution is the greatest challenge for modern extragalactic astrophysics. A huge variety of physical processes are involved in galaxy shaping, and it is a key problem to select the dominant agents driving the evolution of galaxies of different morphological types.

Lenticular galaxies were introduced by Edwin Hubble (1936) when proposing his famous morphological scheme, "Hubble's fork," as a hypothetical intermediate type between ellipticals (to the left) and spirals (to the right): the so-called S0s that he placed in the center of "Hubble's fork" possessed large-scale stellar disks as spiral galaxies, but unlike them lacked patchy patterns of H II regions and spiral arms. Their smooth reddish appearance implied their resemblance to elliptical galaxies as concerning the stellar population ages. It has also long been suggested that the intermediate position of the S0s between pure spheroids (elliptical galaxies) and disk-dominated late-type spiral galaxies obliged them to have very large bulges. However, direct photometric decompositions of the digital images of a representative sample of lenticular galaxies have proved that bulges of any size can be met in S0s, from very large to tiny ones (Laurikainen et al. 2010). So the early idea of Sidney van den Bergh (1976) that within Hubble's morphological scheme the S0 galaxies constitute in fact a morphological sequence parallel to the sequence of spiral galaxies, matching their bulge-to-disk ratios at every morphological subtype, now becomes more and more acceptable (Cappellari et al. 2011; Kormendy & Bender 2012). At first glance, this re-forming of the Hubble morphological sequence strengthens the general opinion that S0s may be formed by quenching star formation in the disks of spiral galaxies; this transformation step must be easier to do when the bulge-to-disk ratios are the same in the progenitor and the descendant. But at this point we would like to note that if the bulges of S0s and spirals are indeed similar, the possibility of obtaining a spiral galaxy from an S0 progenitor arises, whereas this direction of evolution was excluded when the bulges of S0s were supposed to be systematically larger than the bulges of spirals.

A great variety of physical processes that can in principle quench star formation in a disk of a spiral galaxy, to transform it into a lenticular one, are currently discussed: a very incomplete list includes direct collisions (Spitzer & Baade 1951; Icke 1985), tides from a cluster/group dark halo potential (Byrd & Valtonen 1990), "harassment"—high-speed encounters between galaxies in dense environments (Moore et al. 1996), ram pressure by the hot intergalactic medium (Gunn & Gott 1972; Quilis et al. 2000), and starvation of star formation because the external gas reservoir is removed (Larson et al. 1980; Shaya & Tully 1984). All of these processes are inevitably related to dense environments: it is suggested that only clusters and rich groups of galaxies, having massive dark halos enclosing many individual galaxies, can provide the necessary density of the intergalactic medium for an effective ram pressure and the galaxy tight packing for effective gravitational tides. On one hand, indeed, S0 galaxies are known to be the dominant galaxy population of nearby clusters, their fraction in clusters reaching 60% (Dressler 1980). On the other hand, there is an even larger number of S0 galaxies in the field: the galaxy content of the nearby universe

* Based on observations made with the Southern African Large Telescope (SALT), programs 2011-3-RSA_OTH-001, 2012-1-RSA_OTH-002 and 2012-2-RSA_OTH-002.

includes 15% lenticulars (Naim et al. 1995). Some quite isolated lenticular galaxies even exist (Sulentic et al. 2006). What are the mechanisms of their formation? Can be they quite different from those acting in dense environments? This question has not even been considered.

Despite the obvious scarcity of possible galaxy transformation mechanisms beyond the clusters and rich groups, it would be erroneous to think that an isolated galaxy evolves as a "closed box." Recently, we studied an isolated early-type spiral galaxy, NGC 7217. By analyzing the full complexity of its properties, including disk structure, dynamical state, inner gas polar disk, and stellar population characteristics along the radius, we have shown that its present structure requires at least two satellite infalls (minor merging) for the last 5 Gyr (Sil'Chenko et al. 2011). A noticeable gas presence in S0s is not rare, and, in particular, off-cluster environments have appeared to favor an external (accretion) origin of this gas (Davis et al. 2011). Moreover, we have shown that in extremely sparse environments, namely, in the quite isolated S0s, the warm extended gas is *always* accreted from outside (Katkov et al. 2014a). So external gas acquisition, related to smooth cold-gas accretion or to merging small late-type, gas-rich satellites, together with the inner cold-disk instabilities, remains the only possible driver of isolated lenticular galaxy formation and evolution. Taking this idea in mind, we have undertaken a study of the kinematical and stellar population properties of *isolated* lenticular galaxies, hoping to single out the evolutionary paths related just to the gas/satellite accretion regime. Here we must also note that the gas accretion or minor merging allowed for the field disk galaxies are able not only to quench star formation in a large-scale disk, but also to feed and provoke it in the disks where it has not proceeded before (e.g., Birnboim et al. 2007; Sancisi et al. 2008).

To achieve this goal, we have compiled a list of strictly isolated nearby ($v_r < 4000$ km s^{-1}) lenticular galaxies and have undertaken deep long-slit spectroscopy of a small representative sample of them to study the kinematics of the stars and of the gas and the ages and chemical compositions of the stellar populations, as well as the ionization mechanisms and metallicity of the warm-gas component. With these results in hand, we hope to restore the formation and evolutionary histories of the isolated lenticular galaxies. In this paper we show and analyze the data on the southern part of the sample: the galaxies observed at the Southern Africa Large Telescope (SALT) are presented. The paper is organized as follows: Section 2 describes the sample, Section 3 gives the description of the observations and data reduction, in Section 4 we present our results and discuss them in Section 5, and the conclusions drawn from this study are summarized in Section 6.

2. SAMPLE SELECTION

Our approach to compiling a sample of strictly isolated lenticular galaxies is based on a set of methods developed in the Laboratory of Extragalactic Astrophysics and Cosmology of the Special Astrophysical Observatory of the Russian Academy of Sciences by Igor Karachentsev, Dmitry Makarov, and their coauthors. They proposed a new group-finding algorithm that was intended to be applied to their Nearby Galaxy Catalog (Karachentsev et al. 2004, 2013). By extending their study of the local large-scale structures, they have also used their algorithms to identify galaxy pairs (Karachentsev & Makarov 2008), triplets (Makarov & Karachentsev 2009), groups (Makarov & Karachentsev 2011), and isolated galaxies (Karachentsev et al. 2011) up to Hubble velocities of $v_r \leqslant 4000$ km s^{-1}. The updated HyperLEDA and NED databases, extended by measurements coming from the surveys SDSS, 6dF, HIPASS, and ALFALFA, provided line-of-sight systemic velocities, apparent magnitudes, and morphological types of the galaxies under consideration. The benefit of their group-finding approach is that the individual properties of galaxies, in particular an integrated luminosity in the K band as a stellar mass proxy, are taken into account. They assumed that the velocity difference and visible separation of galaxies belonging to a physical pair must both satisfy the condition of negative total energy, and the pair components must be enclosed within the sphere of "zero velocity," which means that the pair components are separated from the Hubble expansion flow. This algorithm for galaxy grouping is iterative: galaxy–galaxy physical pairs are identified during the first iteration, and in subsequent iterations the galaxy pairs are tied into groups through the common members. The isolation index (II) characterizing the isolation degree of any galaxy within the sphere of $v_r \leqslant 4000$ km s^{-1} is a by-product of all of the galaxy grouping procedures. The II value of an unbound galaxy pair is larger than one and indicates a factor by which the mass of one of the components should be increased in order to create a gravitationally bound pair. Correspondingly, the II values of the galaxies belonging to multiple systems are less than one.

Dmitry Makarov has kindly provided us with the information about the isolation indices for all galaxies of the Local Supercluster and its surroundings. To define our sample of isolated lenticular galaxies, we have selected early morphological types, $-3 \leqslant T \leqslant 0$, with the isolation indices II > 2.5. We have also taken some galaxies having faint companions with $1 <$ II < 2.5 but with a K magnitude difference of 3 mag and larger, keeping in mind that the low-mass satellites, with a mass of 10% or less relative to their host, cannot gravitationally affect the evolution of their hosts (unless they merge). The whole sample of isolated lenticular galaxies, from both the northern and southern skies, lists 281 objects. We have started spectral observations of a representative part of this sample. First, we carried out spectroscopic observations of 12 northern targets from the sample of isolated S0 galaxies at the 6 m Russian telescope by using the universal SCORPIO spectrograph; the results are published in Katkov et al. (2014a, 2014b). In this paper we present the results of the long-slit spectroscopic study of nine targets of the southern hemisphere undertaken at the Southern African Large Telescope. As a discussion, a summary of the results for the unified sample of northern and southern isolated S0s is also given at the end of the paper.

3. LONG-SLIT SPECTROSCOPY

3.1. Observations and Data Reduction

The observations were performed with the Robert Stobie Spectrograph (RSS; Burgh et al. 2003; Kobulnicky et al. 2003) at the SALT (Buckley et al. 2006; O'Donoghue et al. 2006). The long-slit spectroscopy mode of the RSS was used with a 1.25 arcsec slit width for most observations. The total time of one observational block with the SALT is limited by the track time of about an hour for our targets. For this reason and because the SALT is a queue-scheduled telescope, most of our galaxies were observed more than once, and all observations

Table 1
Long-slit Spectroscopy of the Studied Galaxies

Galaxy	Date	Exp. (s)	Binning	Slit (arcseconds)	PA (slit) (deg)	Seeing (FWHM, arcsec)
IC 1608	07.11.2012	620 × 3	2 × 4	1.25	350	2.0
	04.01.2013	620 × 3	2 × 4	1.25	350	2.0
IC 4653	11.05.2012	1200 × 3	2 × 2	1.25	52	2.0
NGC 1211	05.10.2011	820 × 3	2 × 2	1.25	210	3.0
	22.11.2011	900 × 3	2 × 2	1.25	210	3.0
	22.12.2011	1030 × 2,730	2 × 2	1.25	210	3.0
	25.12.2011	1000 × 3	2 × 2	1.25	210	3.0
NGC 2917	17.12.2012	900 × 2	2 × 4	1.25	169	3.0
	06.01.2013	900 × 3	2 × 4	1.25	169	3.0
	15.01.2013	900 × 3	2 × 4	1.25	169	3.0
	15.02.2013	900 × 2,700	2 × 4	1.25	169	3.0
NGC 3375	17.02.2012	850 × 2,472	2 × 2	1.25	130	2.0
	23.02.2012	800 × 3	2 × 2	1.25	130	2.0
	28.02.2012	800 × 3	2 × 2	1.25	130	2.0
NGC 4240	14.01.2013	600 × 3	2 × 4	1.25	283	2.0
	19.03.2013	600 × 3	2 × 4	1.25	283	2.0
NGC 6010	05.04.2013	750 × 3	2 × 4	1.00	105	2.0
NGC 7693	10.07.2012	650 × 3	2 × 2	1.25	210	2.0
	04.09.2012	650 × 3	2 × 2	1.25	30	2.0
	22.09.2012	650 × 3	2 × 2	1.25	30	2.0
UGC 9980	10.06.2012	700 × 3	2 × 2	1.25	175	2.0
	10.07.2012	650	2 × 2	1.25	175	2.0

were done during different nights. All of the observational details are summarized in Table 1. The slit was oriented along the major axis for every galaxy except NGC 7693. The grating GR900 was used for our program to cover the spectral range of 3760–6860 Å with a final reciprocal dispersion of ≈0.97 Å pixel^{-1} and an FWHM spectral resolution of 5.5 Å. The seeing during observations was in the range of 1.5–3.0 arcsec. The RSS pixel scale is 0.″1267, and the effective field of view is 8′ in diameter. We utilized a binning factor of two or four to give a final spatial sampling of 0.″258 and 0.″507 pixel^{-1}, respectively. The spectrum of an Ar comparison arc was obtained to calibrate the wavelength scale after each observation, and spectral flats were observed regularly to correct for the pixel-to-pixel variations. Spectrophotometric standard stars were observed during twilights, after observation of objects, for the relative flux calibration.

Primary data reduction was done with the SALT science pipeline (Crawford et al. 2010). After that, the bias- and gain-corrected and mosaicked long-slit data were reduced in the way described in Kniazev et al. (2008). The accuracy of the spectral linearization was checked using the sky line [O I] λ5577; the rms scatter of its wavelength measured along the slit is 0.04 Å. The slit length is approximately 8′, so sky spectra from the slit edges were used to estimate the background during the galaxy exposures.

3.2. The Lick Index System at the SALT/RSS

To derive stellar population properties from the integrated absorption-line spectra of a stellar system, in particular of a galaxy or its part, one can use the equivalent widths (EWs) of the stellar absorption spectral lines. The Lick index (Faber et al. 1985; Worthey et al. 1994; Worthey & Ottaviani 1997) is a uniform, strictly established system of set line parameters measured in part as EWs of strong absorption lines in the spectral range of 4000–6200 Å. The system is named after a 20 year spectral survey of nearby galaxies and stars with the 3 m Lick telescope using a photon-counting detector IDS at the Cassegrain spectrograph. The line and continuum border definitions within the Lick system are tied to the spectral resolution of the Lick spectrograph, ≈8 Å but slightly varying with wavelength. The aim was to fully include the spectral lines in the integrated spectral ranges. The necessity to apply the Lick definitions of the absorption-line EW measurements to galactic spectra was strengthened by the fact that many evolutionary synthesis models of simple stellar populations (SSPs), starting from the work of Worthey et al. (1994), used calibrations of the *stellar* Lick indices on the stellar effective temperatures and metallicities as their input data. These calibration relations were obtained from observations of more than 460 nearby stars with exactly the same Lick spectral setup.

The Volume Phase Holographic (VPH) grating of 900 g mm^{-1} of the SALT/RSS has a spectral resolution of about 5.5 Å that differs from the standard Lick resolution, ≈8 Å. We hence need to calibrate the instrumental absorption-line indices obtained from the RSS spectra by integrating the spectral fluxes in the bands prescribed by the Lick system to the standard Lick system. This was done by observing a sample of Lick standard stars visible in the southern sky from the list of Worthey et al. (1994). In total, 10 giant and dwarf stars with spectral types between F4 and K4 were observed with the VPH900 grating and a slit width of 1.25 arcsec. All of the

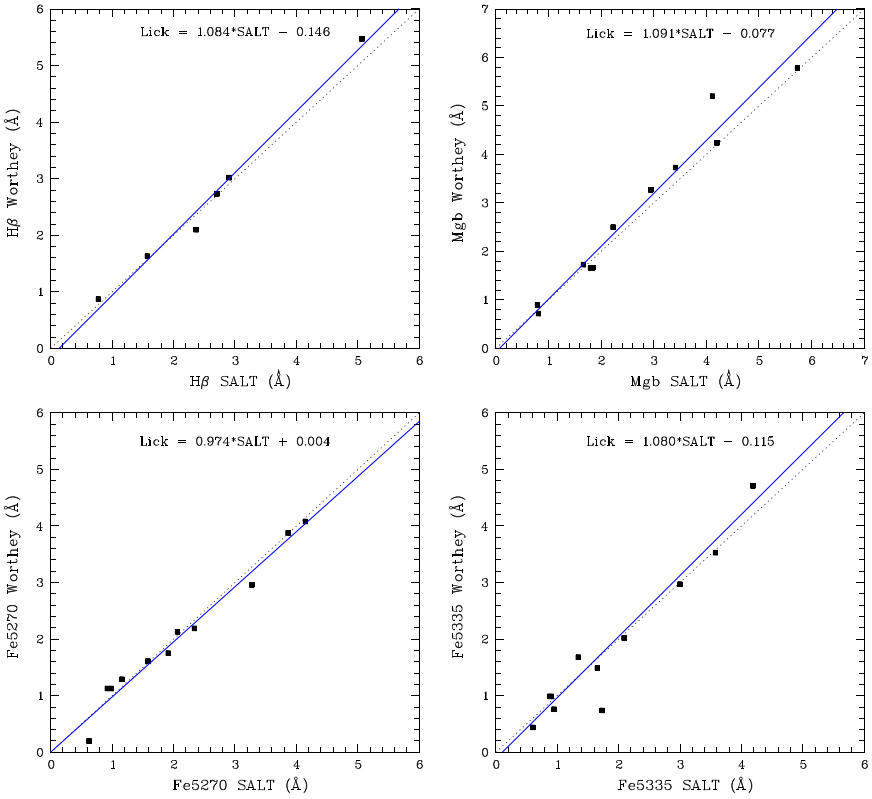

Figure 1. Calibration of the instrumental Lick indices of the RSS/SALT with grating VPH900 onto the standard Lick system. The straight solid lines are the best-fit relations, and the dashed lines are the equality relations.

observations of these bright stars were done either within twilight time or during bright moon time with poor seeing and cloudy conditions. For all of the obtained spectra, we calculated the instrumental-system Lick indices Hβ, Mgb, Fe5270, and Fe5335, by integrating fluxes within the prescribed wavelength intervals for the lines, as well as their blue and red continuum points, as recommended by Worthey et al. (1994).

The instrumental-system Lick indices were then compared to the tabular values provided by Worthey et al. (1994). The linear dependencies between the two sets of data were recovered, and the linear regressions were calculated and are also shown in Figure 1:

$$\mathrm{H}\beta(\mathrm{Lick}) = (1.084 \pm 0.060) \times \mathrm{H}\beta(\mathrm{RSS}) - (0.146 \pm 0.158),$$

and the rms scatter of the points around the straight line is 0.20 Å;

$$\mathrm{Mgb}(\mathrm{Lick}) = (1.091 \pm 0.069) \times \mathrm{Mgb}(\mathrm{RSS}) - (0.077 \pm 0.189),$$

and the rms scatter of the points around the straight line is 0.34 Å;

$$\mathrm{Fe5270}(\mathrm{Lick}) = (0.974 \pm 0.053) \times \mathrm{Fe5270}(\mathrm{RSS}) + (0.004 \pm 0.113),$$

and the rms scatter of the points around the straight line is 0.20 Å;

$$\mathrm{Fe5335}(\mathrm{Lick}) = (1.080 \pm 0.059) \times \mathrm{Fe5335}(\mathrm{RSS}) - (0.115 \pm 0.116),$$

without HD 10700, with the remaining nine stars, the rms scatter of the points around the straight line is 0.22 Å.

Comparing the derived rms scatter of the individual stars around the best-fit straight lines with the mean accuracy of the tabular Lick indices mentioned by Worthey et al. (1994), namely 0.22 Å for Hβ, 0.23 Å for Mgb, 0.28 Å for Fe5270, and 0.26 Å for Fe5335, we conclude that the scatter of the points in the plots of Figure 1 is produced mostly by the errors of the tabular indices.

3.3. Full Spectral Fitting

Besides the Lick index measurements, we have also applied a full spectral fitting approach to our spectra; it is valuable when strong emission lines are present in spectra and the age-sensitive index Hβ is strongly contaminated by the Balmer emission.

In order to perform a full spectral fitting of the synthetic spectra to the observed data, we have used an IDL-based package NBursts (Chilingarian et al. 2007a, 2007b). This package implements a pixel-space fitting algorithm, which involves a nonlinear least-squares optimization using the Levenberg–Marquardt algorithm. The observed spectrum is approximated by a stellar population model broadened by a line-of-sight velocity distribution (LOSVD); the parameters of the stellar population model, metallicity and age, are determined during the same minimization loop as the internal kinematical parameters—the line-of-sight velocity and the stellar velocity dispersion.

In our study, we use intermediate spectral resolution ($R = 10{,}000$) SSP models generated by evolutionary synthesis code pegase.hr (le Borgne et al. 2004) in a wavelength range 3900–6800 Å for the Salpeter (1955) initial mass function based on the ELODIE3.1 stellar library (Prugniel et al. 2007).

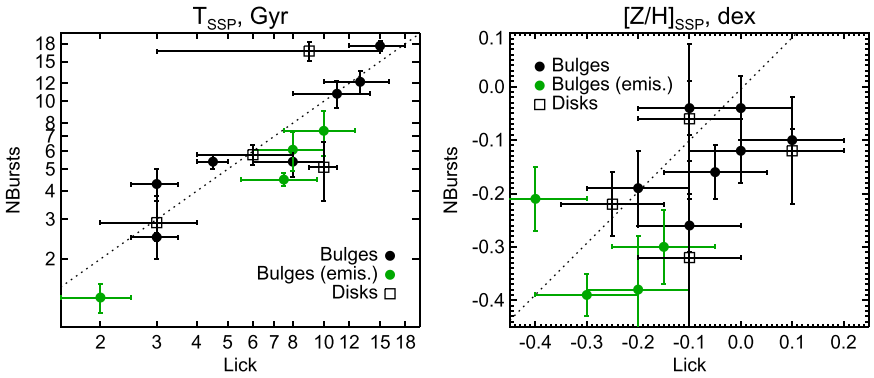

Figure 2. Comparison of the ages and metallicities derived by two different methods: by full spectral fitting using the PEGASE stellar population models ("NBursts") and through the Lick indices Hβ and [MgFe] using the models by Thomas et al. (2003). The dotted line represents the equality locus. The filled circles correspond to measurements in the bulges, and open squares to disks. The green circles show bulges with the presence of emissions in the spectra.

The grid of the synthetic SSP spectra was preconvolved with the spectral line spread function (LSF) of the RSS spectrograph, which was determined by fitting the spectrum of one of the Lick standard stars against the $R = 10{,}000$ spectrum for the same star taken from the ELODIE3.1 library. During the main minimization loop, the template spectrum is extracted from the grid of models by interpolation to the current age T and metallicity [Z/H]. Then the template is convolved with the LOSVD, which is defined by a Gauss–Hermite series of orthogonal functions with parameters v, σ, h_3, and h_4 (van der Marel & Franx 1993). The model includes a multiplicative continuum aimed at taking into account flux calibration uncertainties both in observations and in the models, as well as possible dust attenuation of the galactic spectrum.

In order to avoid systematic errors in the solution, we masked narrow 15 Å–wide regions around ionized-gas emission lines and around traces of the subtracted strong air glow lines. As shown by Chilingarian et al. (2007a) and Chilingarian (2009), excluding age-sensitive Balmer lines from the full spectral fit neither biases age estimates nor significantly degrades the quality of the age determination. To achieve the required signal-to-noise ratio (S/N) of 20–30 per spatial bin, we performed adaptive binning of the long-slit spectra along the slit.

A number of similar approaches to the full spectral fitting techniques exist, for instance PPXF by Cappellari & Emsellem (2004), STARLIGHT by Cid Fernandes et al. (2005), STECKMAP by Ocvirk et al. (2006), and other packages. The main difference between the NBURSTS package and the current version of the popular PPXF code as well as STARLIGHT and STECKMAP is that NBURSTS specifies a template spectrum as a single SSP spectrum with age and metallicity as free parameters. Other packages construct a template spectrum as a linear combination of SSPs with fixed ages and metallicities and SSP weights taken as free parameters. In these cases, the star-formation history can in principle be derived from the observed galaxy spectra, but that requires very high signal-to-noise spectra (Ocvirk et al. 2006). Indeed, the insufficient signal-to-noise level of the spectra leads to degeneracy between weights of the different SSPs and unreliable star-formation history. Due to understanding this effect, the majority of studies where a linear combination of SSPs are used provide only mass- or light-weighted SSP-equivalent parameters of stellar populations that correspond to NBURSTS fitting the parameters by definition.

3.4. Final Choice of the Stellar Population Parameters

To derive the stellar population parameters, we tried both approaches: we fitted "pixel by pixel" all of our spectra along the slit, and we calculated the Lick indices Hβ, Mgb, Fe5270, and Fe5335. The full spectral fitting included the use of the evolutionary synthesis code PEGASE.HR (le Borgne et al. 2004). The measured Lick indices were compared to the models by Thomas et al. (2003), allowing an analysis of magnesium-overabundant stellar populations. To obtain the stellar magnesium-to-iron ratios, we were restricted to the use of the Lick indices only because the full spectral fitting assumed solar abundance ratios. On the other hand, the full spectral fitting has a great advantage in deriving the stellar population ages when we deal with spectra containing strong Balmer emission lines: when the Lick index Hβ is contaminated by the hydrogen emission line, the full spectral fitting is much more safe because it allows one to exclude spectral ranges polluted by emission lines. By calculating the Lick index Hβ, we tried to correct it for the emission by applying our approach based on the measurements of the Hα emission-line EW (Sil'chenko 2006); however, when the emission is strong and the ionized-gas excitation is uncertain, the correction cannot be perfect. Unfortunately, among our southern sample of isolated S0s, almost all of the galaxies demonstrate rich emission-line spectra. So for the present sample in particular we shall analyze mostly the results on the ages and metallicities obtained through the full spectral fitting. However, we wonderered if the two approaches give consistent results, and for a few of our galaxies with weak or absent emission lines, we have compared the ages and metallicities of the bulges and disks obtained by a full spectral fitting using the PEGASE stellar population models with those obtained through the Lick indices Hβ and [MgFe] using the models by Thomas et al. (2003). To get a sufficient statistical level for the comparison, we have included the results for our previous sample of the northern isolated S0s (Katkov et al. 2014b), and the final comparison can be inspected in Figure 2. The ages are consistent within the accuracy of their determination, and the metallicities may have a systematic shift by some 0.1 dex, perhaps due to the slightly nonsolar magnesium-to-iron ratios of the stellar populations in the S0s we studied.

3.5. Ionized Gas

A warm-gas emission-line spectrum can be obtained by subtracting the stellar component contribution (i.e., the best-fitting stellar population model) from the observed spectrum at every spatial bin. The resulting pure emission-line spectra are uncontaminated by absorption lines of the stellar components, which is especially important for the Balmer lines. Then we fitted the emission lines with Gaussians preconvolved with the instrumental LSF in order to determine the LOS velocities of the ionized-gas and emission-line fluxes.

4. RESULTS

By applying the above-mentioned techniques to every galaxy spectrum along the major axis, we have derived the radial profiles of the following characteristics: stellar rotation velocity, stellar velocity dispersion, SSP-equivalent stellar ages, metallicities, magnesium-to-iron ratios, ionized-gas rotation velocity, warm-gas velocity dispersion, and emission-line flux ratios. The latter characteristics can be plotted in the classical excitation-diagnostic diagrams, the so-called BPTs (after Baldwin, Phillips, and Terlevich) (Baldwin et al. 1981), to identify the gas excitation mechanism. If we see that the gas is ionized by young stars, we can apply so-called "strong-line calibrations" to estimate the gas metallicity. We have explored the formulae from the paper by Pettini & Pagel (2004) and have estimated the oxygen abundance using emission-line indices $O3N2 = \log_{10}(([O\,III]\lambda5007/H\beta)/([N\,II]\lambda6583/H\alpha))$ and $N2 = \log_{10}([N\,II]\lambda6583/H\alpha)$, which are calibrated by Pettini & Pagel (2004) against $12 + \log(O/H)$ by using the data on 137 H II regions with known electronic temperatures. In the case of very noisy $H\beta$ and [O III] emission lines, we used another calibration from Pettini & Pagel (2004) that involves only the N2 index. Because of the exploration of ratios of the nearest emission lines, the dust attenuation has no effect on the oxygen abundance estimations.

Below we present the results for every galaxy in a graphical way and give brief descriptions of the individual properties of the galaxies.

IC 1608. This is one of the most luminous galaxies of our sample. The galaxy demonstrates fast stellar rotation; however, the stellar disk is rather hot dynamically, $\sigma_* \geqslant 100$ km s^{-1}. The galaxy is very gas rich: we observe strong emission lines over the full slit extension. The nuclear emission-line spectrum is a typical LINER-like one; starting from the radius of about 10 arcsec, the ionized gas is excited mostly by young stars, and in the outer part, $R \approx 40''$, a star-forming ring is clearly seen. The gas subsystem looks cold only within the star-forming ring; elsewhere in the disk the gas velocity dispersion matches that of stars. The gas rotation curve coincides exactly with the stellar one, so we can be sure that the gas is confined to the main galaxy plane. The gas oxygen abundance at $R > 30''$ is observed to be nearly solar or slightly higher, whereas the stellar mean metallicity there is very poor, about $-0.6 \div -0.9$ dex. The magnesium-to-iron ratio in the stellar component is homogeneous along the radius and close to $+0.1$ dex; the mean stellar age looks intermediate, 3–5 Gyr, over the whole galaxy too. We may thus suspect that low-level star-forming events like the current one have occurred multiple times during the galaxy evolution for the last several billion years; perhaps they have been provoked by small gas-rich satellites merging.

IC 4653. This dwarf galaxy is classified as SB0/a pec in the NED[5] database. However, despite this relatively late morphological type and the elongated isophote shape, our spectrograph slit aligned with the isophote major axis reveals very weak rotation and a rather large stellar velocity dispersion. We would reclassify the galaxy as a dwarf elliptical one and exclude it from further consideration for our sample of isolated lenticular galaxies. Interestingly, the strong emission lines excited by the current star formation are seen over the whole galaxy, including its nucleus.

NGC 1211. This luminous, almost face-on galaxy has a bar and two rings: the inner reddish one at $R \approx 20''$ and the blue star-forming outer one at $R \approx 60''$. Surveys in the 21 cm line earlier reported a large neutral hydrogen content in this galaxy, 5.5 billion solar masses of H I (Garcia-Appadoo et al. 2009), so the strong emission lines were also expected in its optical spectrum. The discrepancy between the rotation velocities of the ionized gas and the stars at $R < 10''$ can be explained both by asymmetric drift and bar influence; beyond the radius of $10''$ the ionized gas and stars rotate together, and we conclude that the gas is confined to the main galaxy plane. The gas is excited by the LINER-like nucleus and by shock waves (from the bar?) in the central part of the galaxy at $R < 10''$, and by young stars beyond this radius; the oxygen abundance of the gas in the outer star-forming ring is the solar one. Meanwhile, the low-surface-brightness stellar disk at $R \approx 30''$ demonstrates very old age, $T \geqslant 10$ Gyr, and very low stellar metallicity, $[Z/H] \approx -1.5$ dex. The bulge and the lens, which we relate to the bar ends, demonstrate intermediate stellar ages and a strong metallicity gradient along the radius.

NGC 2917. This very luminous $S0^+$ galaxy is strongly inclined to the line of sight, but it is not exactly edge-on, so we can distinguish a dust ring and no signs of a bar in the galaxy. The bulge is so small that the galaxy has been included in the list of "flat" late-type galaxies by Mitronova et al. (2004). The systemic velocity of NGC 2917 given in the NED, 3675 km s^{-1}, is erroneous coming from a very weak spurious 21 cm signal detected by Richter & Huchtmeier (1987). Our optical spectral observations give $v_{sys} = 5377$ km s^{-1} for this galaxy, so the galaxy is even more luminous than was thought before. Though we have traced the stellar component of NGC 2917 almost up to its optical border, $R_{25} = 38''$ (RC3),[6] we have only measured its lens; the outer stellar disk is a very low-surface-brightness one and could not be detected in our observations. While the bulge has intermediate stellar-population characteristics, the lens looks rather young, $T = 2$–3 Gyr, which is consistent with the ionized gas excited by current star formation at $R \geqslant 10''$. The ionized-gas metallicity is high. The fall of the ionized-gas rotation velocity at the southern edge of the galaxy accompanied by the rise of the velocity dispersion of the gas clouds seems to be real. Are there any traces of interaction?

NGC 3375. Another galaxy that was previously classified as a lenticular one is in fact an elliptical: its stellar component does not rotate regularly, and the stellar velocity dispersion exceeds 150 km s^{-1} everywhere through the galaxy. Emission lines are absent in the spectrum.

NGC 4240. The galaxy is classified in RC3 as between E and S0 ($T = -3.8 \pm 0.5$). In the frame of the Automated Plate Measuring (APM) survey (Naim et al. 1995) when six

[5] NASA/IPAC Extragalactic Database.
[6] Third Reference Catalog of Bright Galaxies.

Table 2
Average Stellar Population Parameters

Galaxy	N(bins)	T, Gyr	[Z/H], dex	[Mg/Fe], dex	σ, km s^{-1}
			Bulge		
IC 1608	4	$4.7^{\pm0.3}$	$-0.21^{\pm0.07}$	$0.12^{\pm0.09}$	$149^{\pm9}$
NGC 1211	3	$4.5^{\pm0.4}$	$-0.16^{\pm0.05}$	$0.11^{\pm0.07}$	$156^{\pm18}$
NGC 2917	4	$6.1^{\pm1.3}$	$-0.21^{\pm0.06}$	$0.27^{\pm0.08}$	$191^{\pm4}$
NGC 4240	4	$4.6^{\pm0.3}$	$-0.32^{\pm0.08}$	$0.18^{\pm0.09}$	$108^{\pm11}$
NGC 6010	4	$8.16^{\pm0.45}$	$-0.19^{\pm0.07}$	$0.19^{\pm0.06}$	$154^{\pm11}$
NGC 7693	8	$1.35^{\pm0.18}$	$-0.38^{\pm0.10}$	$-0.02^{\pm0.02}$	$82^{\pm14}$
UGC 9980	6	$7.4^{\pm1.4}$	$-0.30^{\pm0.07}$	$0.18^{\pm0.11}$	$138^{\pm20}$
			Disk		
IC 1608	8	$3.5^{\pm0.8}$	$-0.46^{\pm0.14}$	$0.18^{\pm0.15}$	$138^{\pm32}$
NGC 1211	2	$10.5^{\pm4.1}$	$-1.50^{\pm0.14}$	...	$141^{\pm12}$
NGC 2917	0	...	...	...	...
NGC 4240	5	$5.4^{\pm2.1}$	$-1.02^{\pm0.11}$	$0.33^{\pm0.13}$	$112^{\pm8}$
NGC 6010	12	$5.4^{\pm2.4}$	$-0.36^{\pm0.16}$	$0.18^{\pm0.04}$	$113^{\pm21}$
NGC 7693	11	$1.5^{\pm0.9}$	$-0.67^{\pm0.21}$	$0.15^{\pm0.13}$	$106^{\pm24}$
UGC 9980	5	$9.8^{\pm2.8}$	$-0.99^{\pm0.12}$	$0.21^{\pm0.20}$	$83^{\pm5}$
			Lens/Ring/Plateu		
IC 1608	10	$4.6^{\pm2.8}$	$-0.77^{\pm0.20}$	$0.24^{\pm0.08}$	$98^{\pm5}$
NGC 1211	12	$5.6^{\pm2.7}$	$-0.82^{\pm0.23}$	$0.20^{\pm0.18}$	$148^{\pm38}$
NGC 2917	10	$2.6^{\pm0.6}$	$-0.34^{\pm0.08}$	$0.24^{\pm0.07}$	$130^{\pm21}$
NGC 4240	0	...	...	...	...
NGC 6010	0	...	...	...	...
NGC 7693	0	...	...	...	...
UGC 9980	7	$4.6^{\pm2.2}$	$-0.48^{\pm0.18}$	$0.22^{\pm0.19}$	$114^{\pm8}$

independent researchers classified it "by eye," three voted for S0 and three voted for E (see the "detailed classification" option in the NED). However, our long-slit cross section along the major axis reveals a rather fast rotation of the stellar component, and in the photometric data we see an exponential disk at $R > 15''$, so we consider NGC 4240 to be a lenticular galaxy. The stellar population properties were spectrally studied by Reda et al. (2007) up to the distance about $10''$ from the center; a slightly subsolar metallicity and a rather old age were measured by the Lick index method. The kinematics was examined by Hau & Forbes (2006); however, their slit was obviously off the dynamical center, and they did not report a gas counterrotation for this galaxy, which is striking. We have traced the stellar rotation and stellar population properties toward $R \approx 25''$, measuring not only the bulge but also the large-scale stellar disk at $R > 15''$. Both the bulge and the disk have an intermediate stellar age, about 5 Gyr, but the disk is very metal poor, [Z/H] ≈ -1.0, and the bulge has only [Z/H] ≈ -0.3. The ionized gas counterrotates the stars in the bulge-dominated area; while the stellar velocity dispersions of the stars and gas clouds are comparable, the rotation velocities differ significantly, and we conclude that the ionized gas may rotate in a plane that does not coincide with the plane of the stellar disk. The gas metallicity in the outer star-forming ring, at $R \approx 15''$, is close to the solar one.

NGC 6010. This is another small-bulge, edge-on S0 galaxy included in the catalog of "flat galaxies" by Mitronova et al. (2004). Also, we must note that in our present sample it is the only S0 galaxy without strong emission lines in the spectra. We see only weak narrow emission lines with LINER-like excitation in the very circumnuclear region; some signs of the ionized-gas counterrotation are however detected. Meanwhile, neutral hydrogen is found in this galaxy by Springob et al. (2005), but no signs of recent star formation are present. The stellar ages of the nucleus ($T = 9$ Gyr) and of the bulge ($T = 8$ Gyr) are slightly older than in other galaxies of our sample. However, the characteristics of the disk in the radius range $R = 20''$–$40''$ are the quite typical –$T = 5$ Gyr and [Z/H]$= -0.4$.

NGC 7693. Because of instrumental problems, the galaxy was observed with the slit turned by some 40° to the major axis. However, even so, the observed stellar rotation is too slow, and the ionized-gas velocities are quite decoupled from the stellar ones. Consequently, no signs of current star formation are seen in this galaxy, though both the bulge and the disk look very young, 1–3 Gyr old. The magnesium-to-iron ratio over the whole galaxy is solar, so it seems that continuous star formation ceased rather recently, perhaps due to just a minor merger from an inclined orbit.

UGC 9980. This galaxy demonstrates fast regular rotation, looking quite similar in the stellar and ionized-gas components. The gas is spread over the whole galaxy, and starting outward from the radius $R > 10''$ it is excited by young stars. However, both the bulge and the large-scale stellar disk possess rather old stellar populations, $T = 7$ Gyr in the former and $T = 10$ Gyr in the latter, so the widespread star formation evidently started quite recently: unlike the case of NGC 7693, this time, minor merging has stimulated star formation, not ceased it. The difference in metallicities—[Z/H] $= -1.0$ dex in the stellar disk and −0.2 dex in the gaseous disk—also indicates the external origin of the current fuel for star formation. The inner stellar ring related to ansae at the ends of the bar, at $R \approx 10''$, is distinguished by a slightly younger stellar age, $T \approx 5$ Gyr. However, this ancient ring-like star-formation burst was

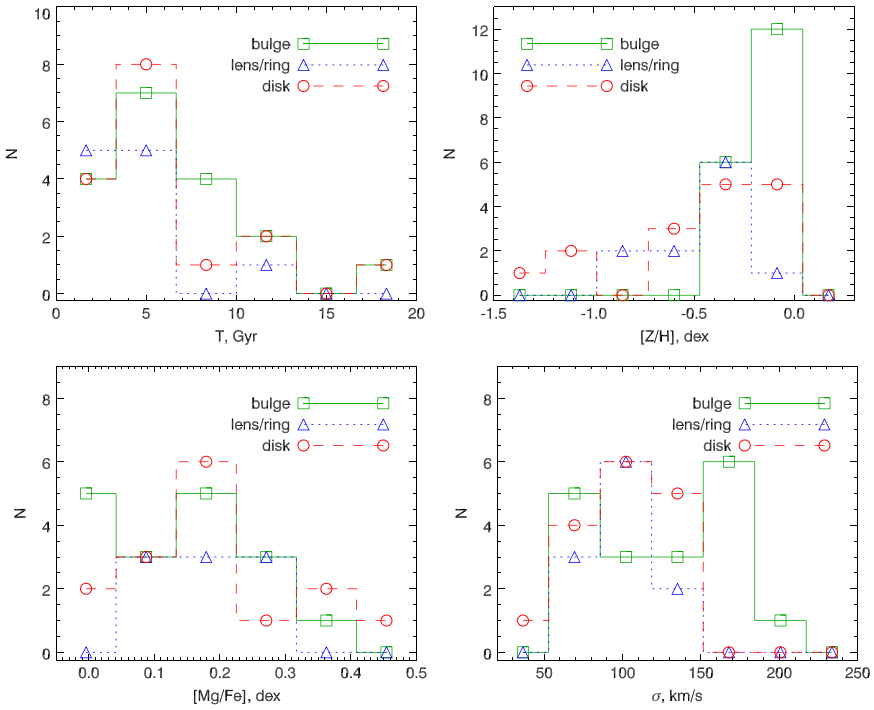

Figure 3. Distributions of our complete sample of the isolated lenticular galaxies over the found parameters of the stellar populations for every structural component: bulges, disks, and rings or lenses.

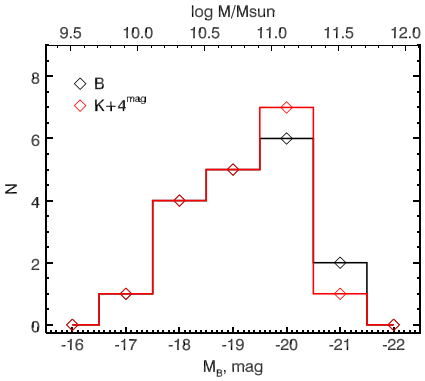

Figure 4. Histogram of integrated absolute magnitudes in the B band (black line) and shifted by 4^m K band (red line) for the total SALT and SCORPIO sample of the isolated lenticular galaxies. The corresponding stellar masses are shown in the upper x axis and were calculated by using $M/L_K = 1$.

probably related not to interaction but to the bar affecting the gaseous disk of the galaxy, which was perhaps more gas rich at $z = 0.5$ than it is at the present epoch.

After obtaining the full radial profiles of the stellar characteristics in the galaxies studied, which are presented in Figures 11–19, we wished to extract the mean characteristics for the large-scale galaxy components—bulges and disks. To identify radius ranges that correspond to the bulge and disk domination in the integrated light, we have undertaken a photometric decomposition of the images of the galaxies. For this purpose, we have used mostly the SDSS public database, Data Release 9; the r-band images as the images with the highest S/N have been taken. For the southern galaxy NGC 4240, which was not observed in the frame of the SDSS, we have decomposed the Two Micron All Sky Survey (2MASS) composite, $J + H + K$, image. For one galaxy, IC 1608, very deep gri photometric data were obtained during test

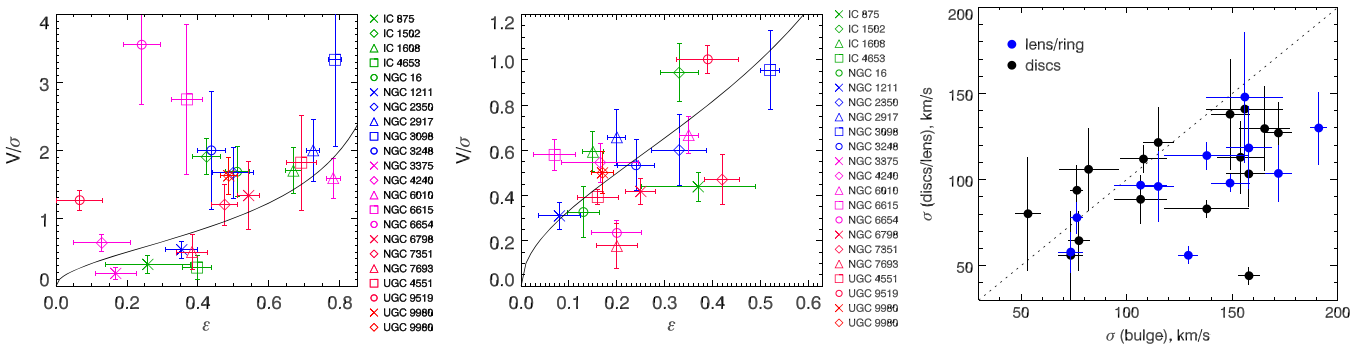

Figure 5. Dynamical diagnostics diagrams: ellipticity versus V/σ for the disks (left), the same for the bulges (center), and a comparison of the stellar velocity dispersions in the bulges and disks (right). The solid line shows the locus of oblate spheroids, which can be considered as a demarcation line between disk-like and spheroid-like systems.

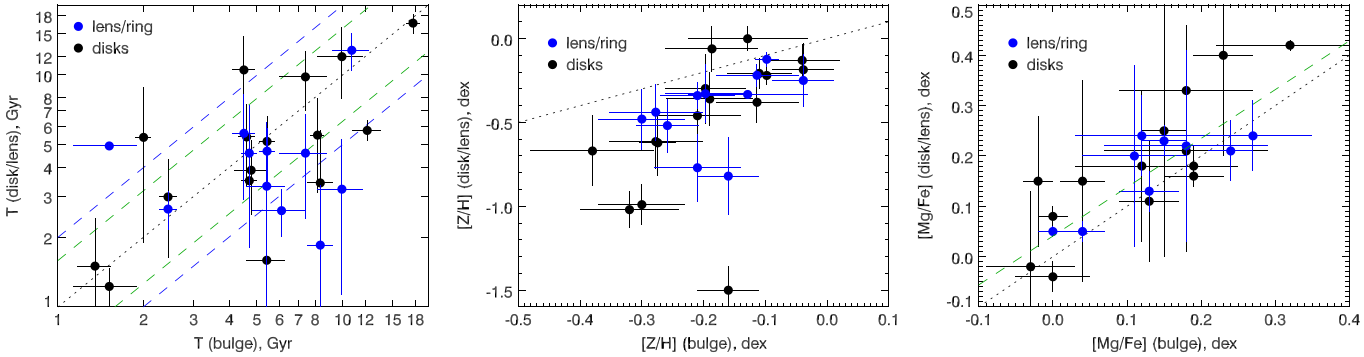

Figure 6. Comparison of the stellar populations in the bulges and in the disks: age–age diagram (left), metallicity–metallicity diagram (center), and [Mg/Fe]−[Mg/Fe] (right). The green and blue dashed lines in the left panel correspond to the deviation from a bisector (dotted line) of value ±0.2 dex (by 1.5 times) and ±0.3 dex (by two times), respectively. The dotted lines show the equality line. The green dashed line in the right panel shows the linear fit of the measurements.

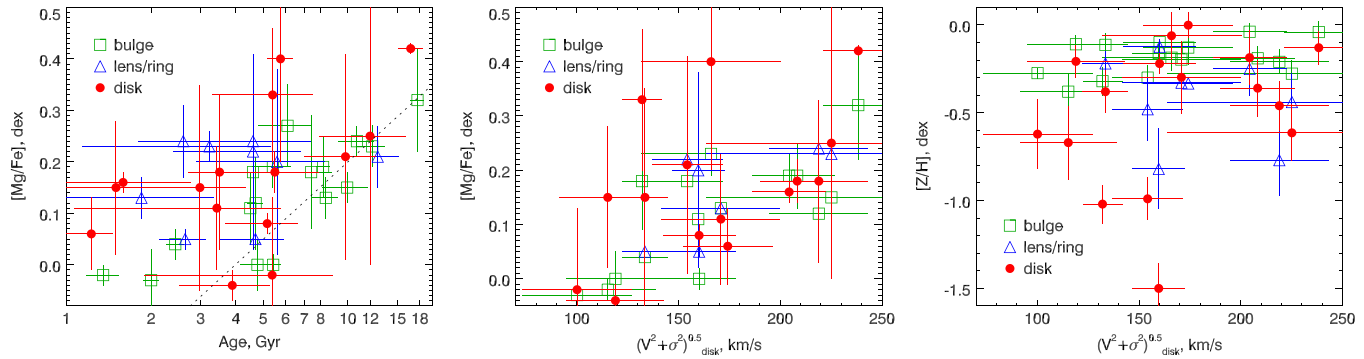

Figure 7. Relation age–Mg/Fe ratio (left), dynamical parameter $(v^2 + \sigma^2)^{0.5}$ versus alpha-element abundance (center), and some kind of mass–metallicity relation (right).

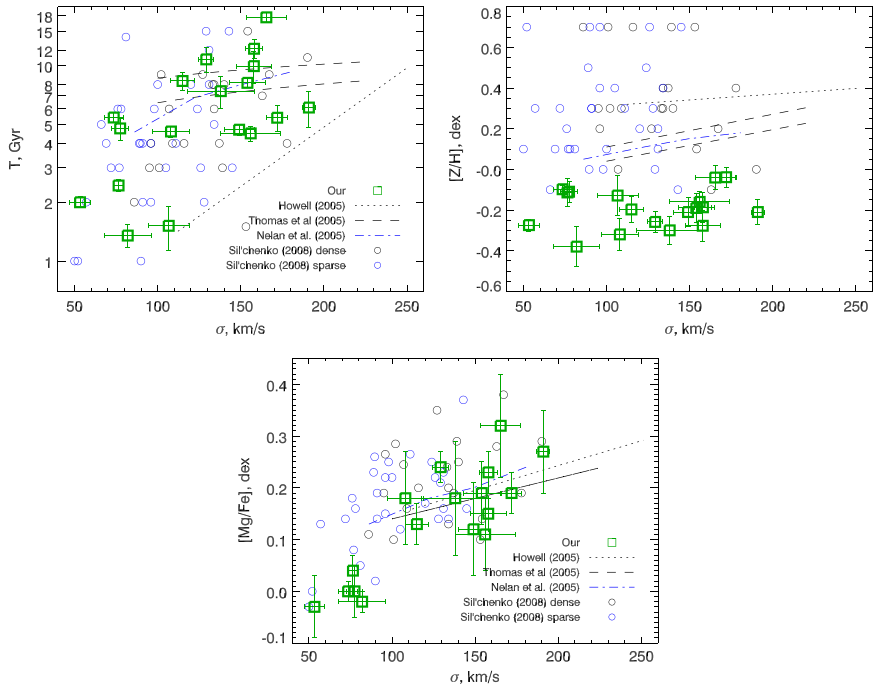

Figure 8. Comparison of the stellar population properties with the stellar velocity dispersion for the bulges of lenticular galaxies. The green squares show our measurements in the isolated lenticulars; circles correspond to measurements from Sil'chenko (2008), and colors indicate the environmental properties of galaxies (black is dense, blue is sparse). Various samples of early-type galaxies from the literature are also shown. For details see Section 5.1.

observations of the LCOGT project (Sil'chenko et al. 2015). For every galaxy, we have performed an isophotal analysis and derived azimuthally averaged surface-brightness radial profiles. By inspecting these profiles, we have found the outer radial segments where the surface-brightness radial profiles can be well approximated by exponential laws and the isophote

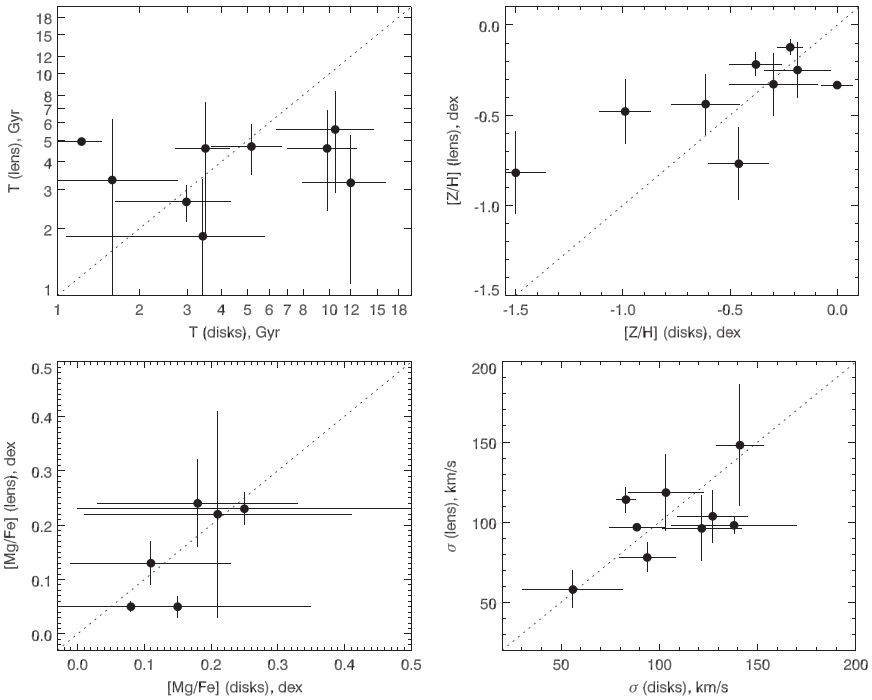

Figure 9. Comparison of the disks and their rings or lenses. The dotted line corresponds to the equality line.

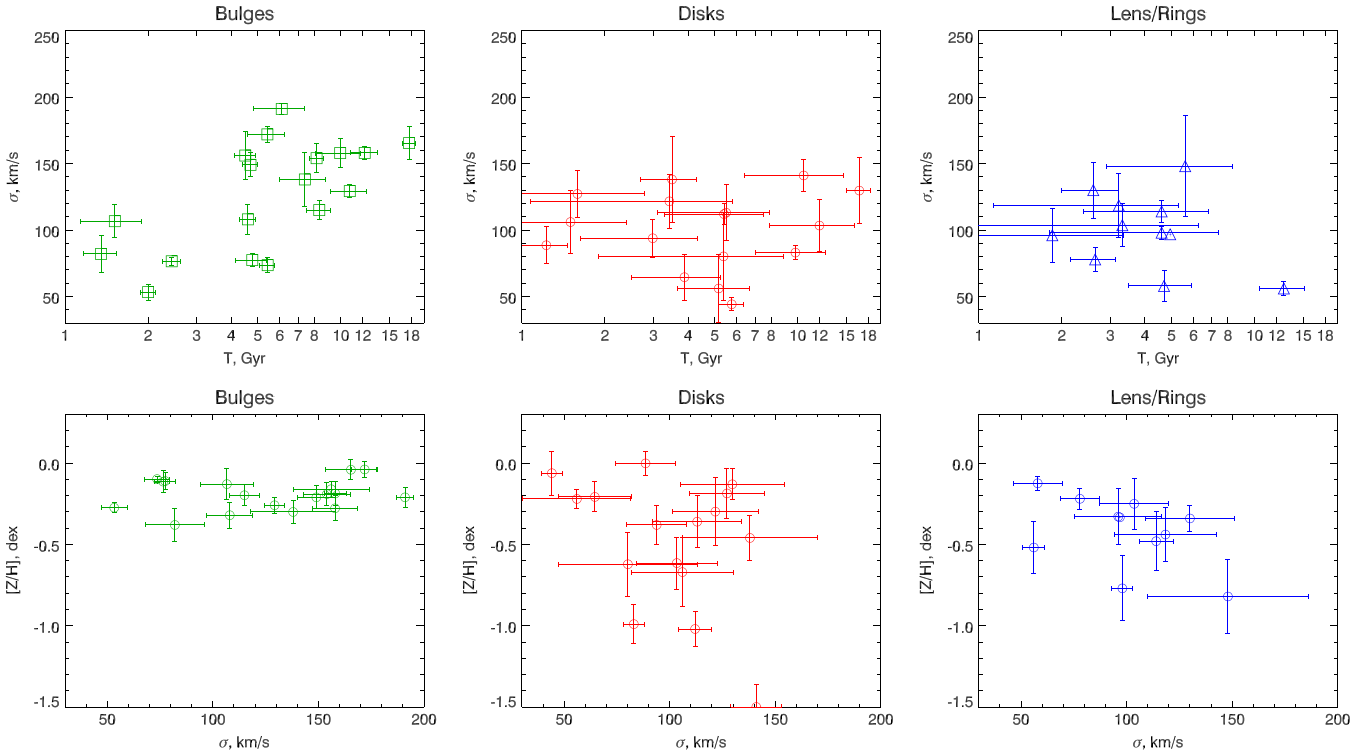

Figure 10. Parameters of the stellar populations for the joined sample SALT and SCORPIO targets.

ellipticity stays constant. These outer parts of galaxies are identified by us as disk dominated. To characterize the bulges that are mostly compact in the galaxies of our sample, we fix the radial range of $4''-7''$ that is beyond the unresolved nucleus contamination under our seeing conditions. In some galaxies, we have also distinguished the radial ranges where we see rings of enhanced stellar brightness or flat brightness profile segments betraying the presence of lenses. The corresponding segments for each component are shown by shaded gray lines in the figures. The mean stellar ages, metallicities, and magnesium-to-iron ratios for the bulges, disks, rings, and lenses of the galaxies studied here are presented in the Table 2.

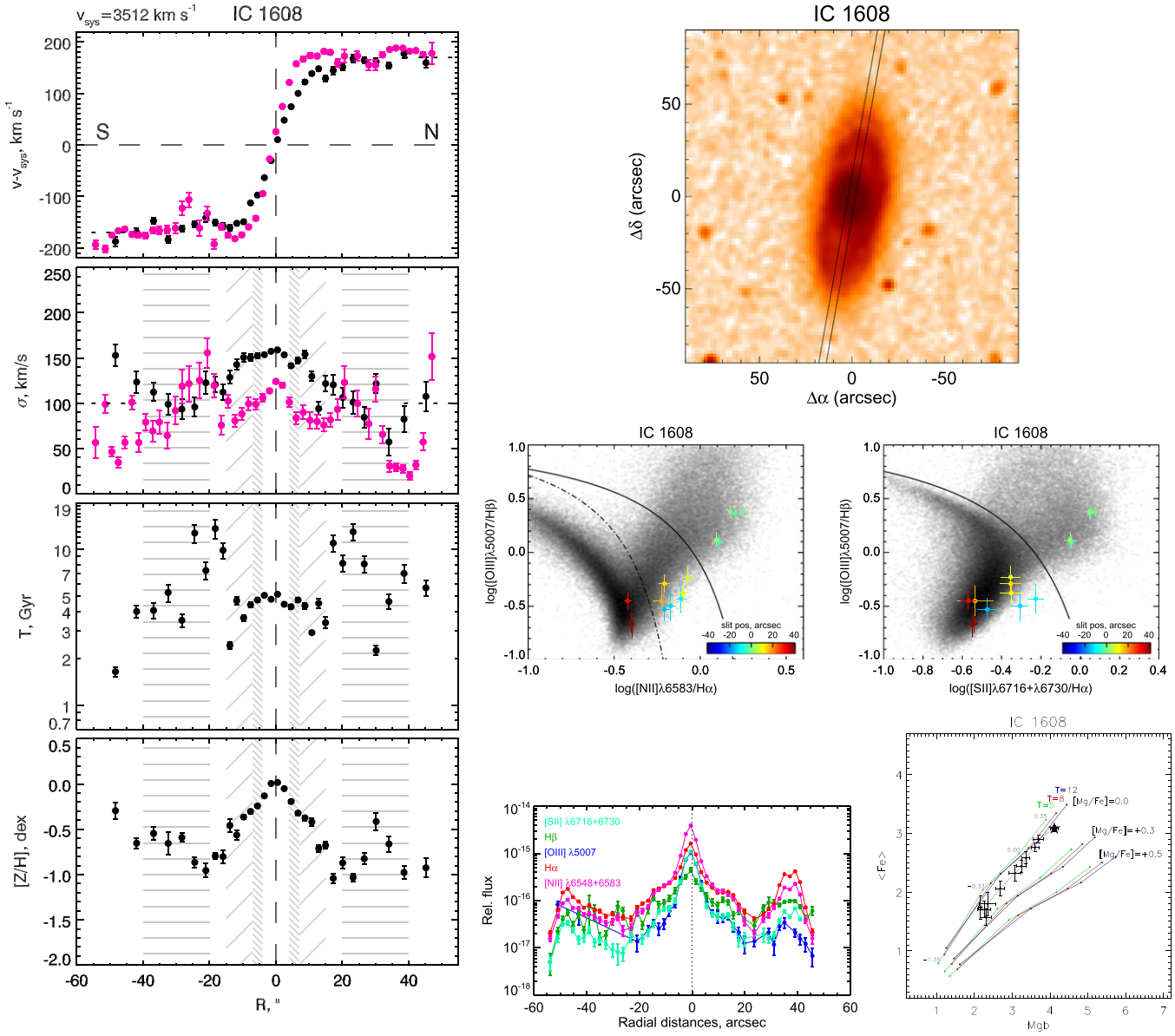

Figure 11. IC 1608. Left block from top to bottom: (i) the radial profile of stellar (black) and gaseous (pink) line-of-sight velocity; (ii) the stellar and gaseous velocity dispersion; (iii) properties of stellar populations: ages and metallicities. The shaded gray lines show radial segments where average stellar population parameters are calculated: "\"-like shading corresponds to bulge dominance regions, "–" to lens/ring regions, and "/" to disk ones. Right block from top to bottom: (i) long-slit position superimposed on a DSS image of the galaxy; (ii) excitation diagnostic diagrams comparing different emission-line ratios. The reference distribution of the measurements of the line ratios for galaxies from the SDSS survey with high S/Ns (S/N > 3 in every line) are shown by the gray color. The black curves, which separate the areas with the AGN/LINER excitations from areas with the star formation–induced excitation, are taken from Kauffmann et al. (2003) (dash-dotted curve) and from Kewley et al. (2006) (solid curve). (iii) Observed emission line fluxes. (iv) Diagnostic diagram ⟨Fe⟩ versus Mgb. Points with error bars represent our measurements along the radius of the galaxy, starting from the nucleus marked by a large star. The SSP models by Thomas et al. (2003) for three different magnesium-to-iron ratios (0.0, +0.3, and +0.5) and three different ages (5, 8, and 12 Gyr) are plotted as reference.

5. DISCUSSION

In this paper, we have described the results of a spectral study for seven isolated lenticular galaxies of the southern sky (another two galaxies observed so far have been reclassified here as ellipticals based on their stellar kinematics and do not take part in the analysis below). Earlier we published the results of a similar study for 11 isolated lenticulars of the northern sky, which were observed at the Russian 6 m telescope using the SCORPIO and SCORPIO-2 spectrograph (Katkov et al. 2014a, 2014b). With the total of 18 isolated lenticular galaxies observed with the long-slit spectrographs of two large telescopes, we can now discuss some statistical properties concerning the kinematics, the stellar population parameters, and the ionized-gas features in isolated lenticular galaxies. The overall distributions of the parameters of the stellar component for the bulges, disks, and rings or lenses are presented for the total sample in Figure 3. The distribution of the absolute magnitudes in the *B* and *K* bands are shown in Figure 4.

5.1. Bulges versus Disks

Figure 5 demonstrates first of all the dynamical status of the bulges and disks in our sample of isolated lenticular galaxies. The diagrams presented in the two left plots for the disks and

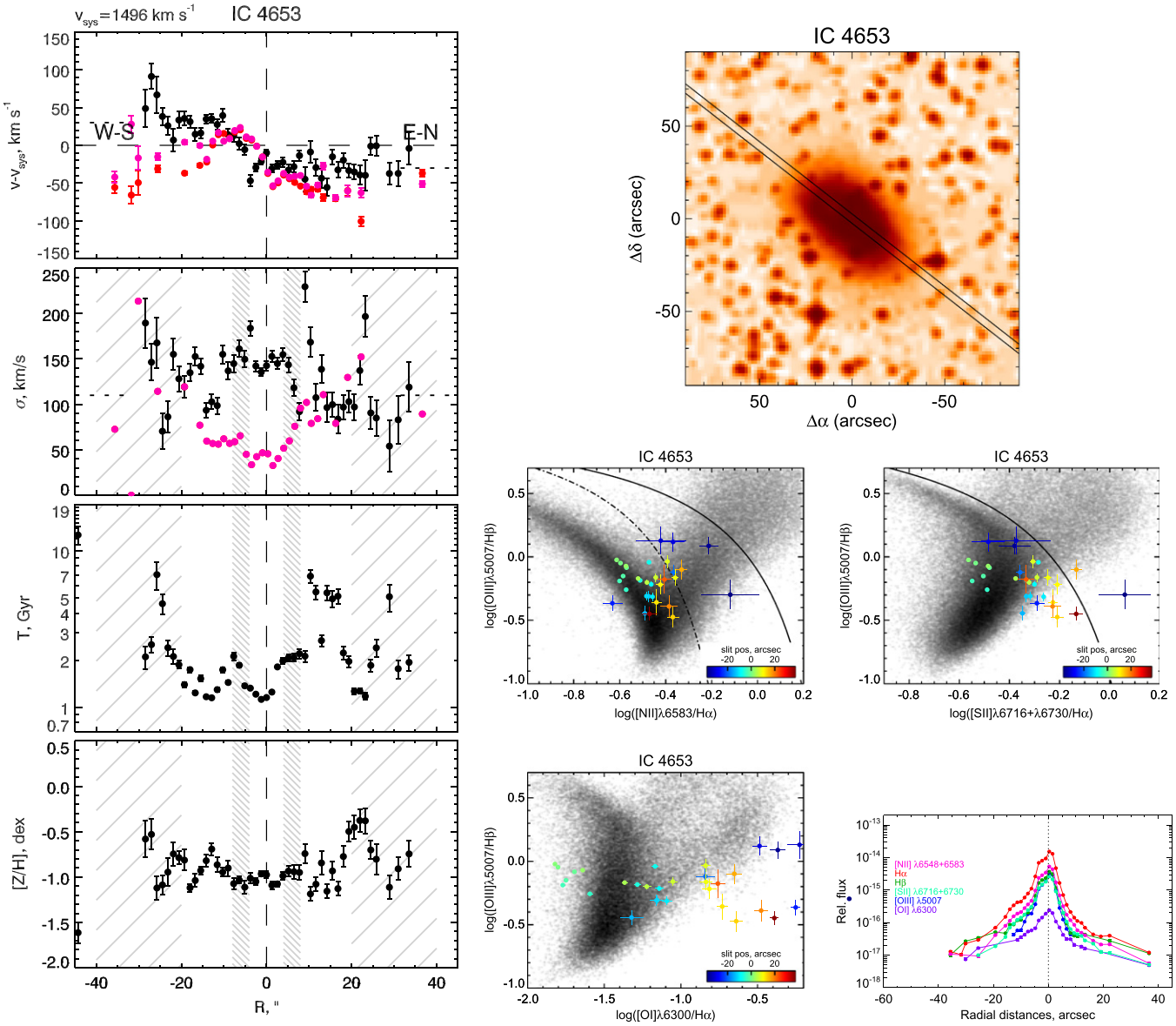

Figure 12. IC 4653. The same as the previous figure.

for the bulges, respectively, compare the ratio of the regular rotation velocity to the stellar velocity dispersion versus the visible ellipticity of the isophotes. It was proposed by Illingworth (1977) and theoretically calculated by Binney (1978b, 1978a) to check if the shape of a galaxy spheroid is supported by rotation. The main theoretical locus in this diagram signifies so-called oblate spheroids—ones round in the equatorial plane, with an isotropic velocity dispersion, whose smaller third axis is completely explained through flattening by rotation. Many true elliptical galaxies are found well below this locus because they rotate too slowly, and their shapes are supported by the anisotropy of the velocity dispersion distributions. John Kormendy (1993) (see also Kormendy & Kennicutt (2004) for the updated version of this diagram) used this diagram for the bulges of disk galaxies to separate so-called "classical bulges," which can be considered as analogs of elliptical galaxies, from the "pseudobulges," which reveal disk-like kinematics. If the observed characteristics place some bulges above the theoretical line for oblate spheroids, we would classify them as "pseudobulges" formed from the disk material during secular dynamical evolution. Figure 5, middle plot, gives evidence for the roughly equal proportion of "classical bulges" and "pseudobulges" among the isolated lenticular galaxies: the points are oscillating around the theoretical locus for the oblate isotropic spheroids. When inspecting Figure 5 (right plot), we confirm again that in 8–10 bulges of the 18 the stellar velocity dispersion is the same as in the surrounding disks, so indeed these are "pseudobulges."

Figure 6 gives a comparison of the characteristics of the stellar populations in the bulges and in the disk structures: it is the comparison of the age–age, metallicity–metallicity, and Mg/Fe ratio–Mg/Fe ratio. The first and third plots demonstrate correlations between the properties of the bulges and of the disks: covering the whole range of possible ages, from 1 to 17 Gyr, the mean stellar ages of the bulges and disks tend to be similar in the galaxies studied, and the magnesium-to-iron ratios are strictly the same in the bulges and in the disk structures. This is in opposition to the properties of S0 galaxies

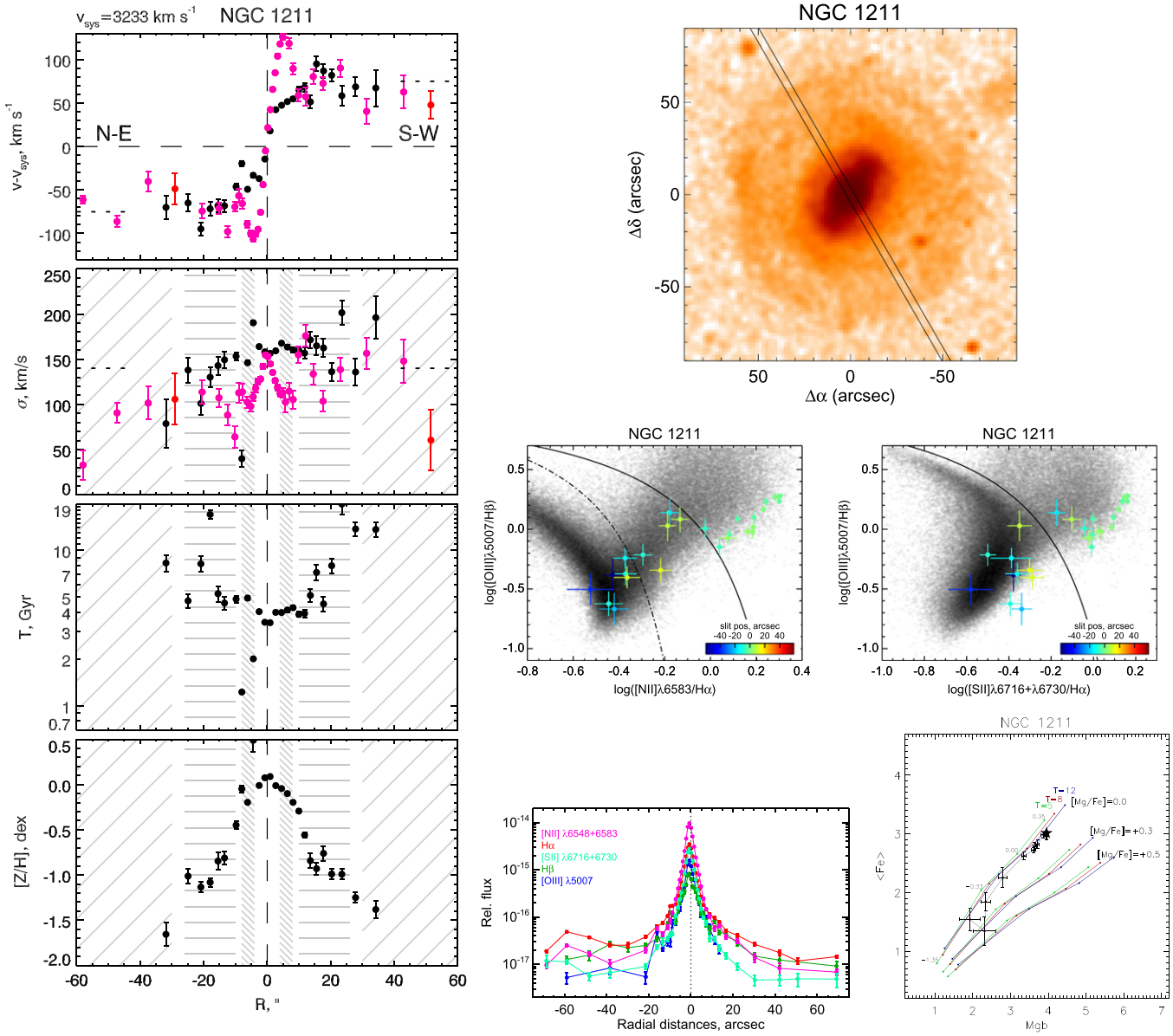

Figure 13. NGC 1211. The same as the previous figure.

in denser environments: Sil'chenko et al. (2012) found for a sample of mostly group S0 members that the disks appear to usually be older than the bulges, covering homogeneously the upper left corner of the diagram, similar to Figure 6 (left plot), and Johnston et al. (2014) have found just the same effect for all of the Virgo S0s they studied. In both dense-environment samples, the stellar disks appear to be much more overabundant in magnesium than are the bulges. We can conclude that when placed beyond the outer gravitational and hot-medium influence, the bulges and the disks in S0 galaxies formed synchronously: star formation started simultaneously here and there and ceased at one moment. Interestingly, despite the synchronous star formation, the mean stellar metallicities of the disk structures are significantly lower than the metallicities of the bulges (Figure 6, middle plot). Does this mean that pristine outer gas was accreted by the outer disks and fueled star formation there, while the nearly simultaneous star formation in the bulges was fed by the gas preprocessed and enriched in the disks?

Let us inspect some scaling relations connecting the evolutionary and dynamical characteristics of the stellar components that are commonly studied for the elliptical galaxies. Figure 7 (left plot) compares the mean stellar ages of the different structural components with their magnesium-to-iron ratio, which characterizes the duration of the main star-forming episode, from very brief, shorter than 10^9 years ([Mg/Fe] $= +0.3$), to several gigayears ([Mg/Fe] $= 0.0$). We see a cloud of points limited at the lower right by a linear law that probably marks the initial epoch of star formation launching in S0s at $z \approx 3$: star formation starting 12 Gyr ago and ceasing immediately would give [Mg/Fe] $= +0.3$, and star formation starting 12 Gyr ago and lasting to 4 Gyr ago would give [Mg/Fe] $= 0.0$. However, there are many points, related both to the bulges and to the disks, that expand to the left of this limiting line. Obviously these are the stellar systems that have started their formation much later than at $z = 2$–3: to get the mean stellar age of 3 Gyr and [Mg/Fe] $= +0.3$ signifying the duration of star formation less than 1 Gyr, the process had to

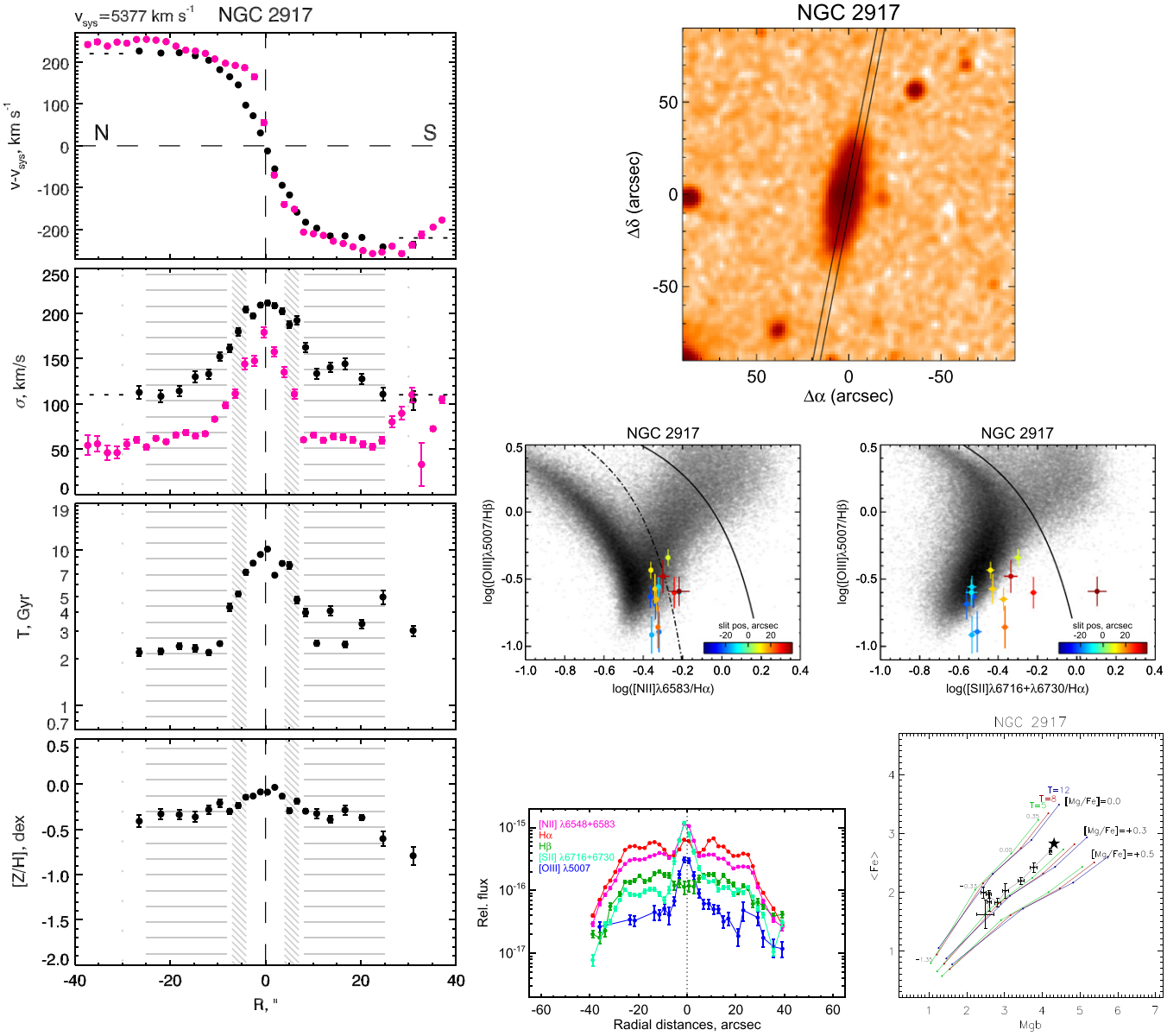

Figure 14. NGC 2917. The same as the previous figure.

be launched at $z = 0.4$. From this plot, we conclude that the main star-formation events both in the bulges and in the disks of the isolated S0 galaxies have no single fixed epoch, but are homogeneously spread from very high redshifts to rather recent ones.

Two other plots in Figure 7 compare the chemical properties of the stellar populations to the dynamical parameter $(v^2 + \sigma^2)^{0.5}$, where v and σ are the rotation velocity and stellar velocity dispersion averaged over the disk-dominated or bulge-dominated area; this dynamical parameter characterizes, under the condition of virialization, the local gravitational potential. The correlation of the magnesium-to-iron ratio with the gravitational potential well, in particular with the central stellar velocity dispersion, is well known for the elliptical galaxies (e.g., Trager et al. 2000). In our data, we see that the bulges (spheroids) and the disks behave similarly regarding the duration (the effectiveness?) of star formation in a particular gravitational potential well: the deeper the well, the shorter duration of star formation. However, the similarity of the bulges and disks disappears when we inspect not the Mg/Fe ratio but the global metallicity versus the dynamical parameter (Figure 7, right plot): while the bulges follow the well-known mass–metallicity relation, the larger the mass, the higher the metallicity, and this correlation vanishes completely for the disks.

We can put our results on the stellar population properties in the bulges of isolated lenticular galaxies into a wider context by referring to the study of nearby lenticular galaxies with the integral-field spectrograph of the Russian 6 meter telescope, Multi Pupil Fiber Spectrograph (MPFS), by Sil'chenko (2006, 2008). In this work (Sil'chenko 2008), the data for the nuclei and bulges of more than 50 nearby S0s were presented; the sample included galaxies over a wide range of environments and was divided into two parts: "dense environments" (Virgo cluster and central galaxies of rich groups) and "sparse environments" (mostly peripheries of groups). In Figure 8 we reproduce the Figure 2 from Sil'chenko (2008), where we overplot our present results on the bulges of

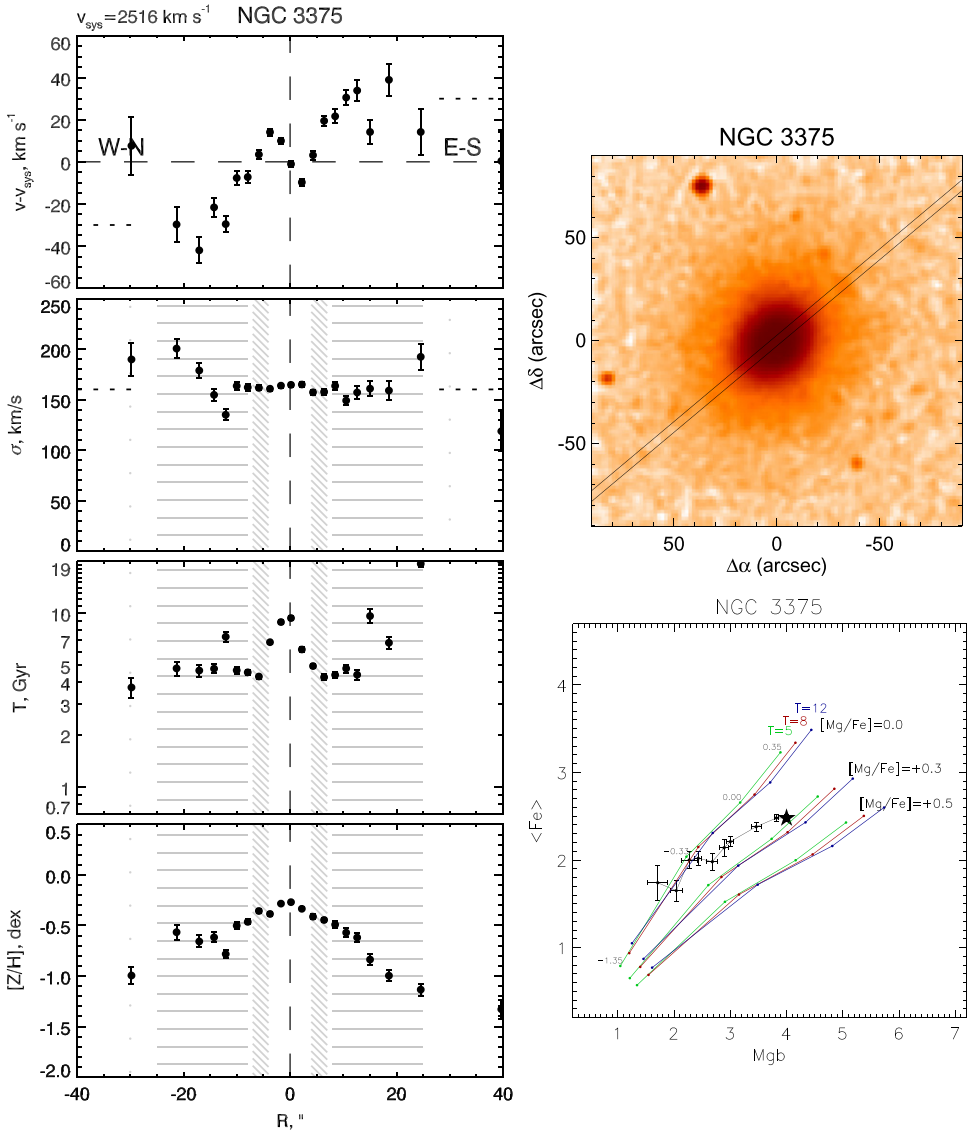

Figure 15. NGC 3375. The same as the previous figure.

completely isolated S0s. Besides the data on the bulges of nearby S0s, this figure also contains the mean relations for the integrated stellar population properties of elliptical galaxies in clusters (Nelan et al. 2005), in the field (Howell 2005), and in both types of environments (Thomas et al. 2005). We must note here that among these comparison samples only ellipticals were considered by Howell (2005); Nelan et al. (2005) and Thomas et al. (2005) have mixed ellipticals and lenticulars. In Figure 8 we see that the relations connecting the ages and the [Mg/Fe] ratios with the stellar velocity dispersion found for spheroids in a wide range of environments are broadly consistent with our results on the bulges of isolated lenticular galaxies. However, the stellar metallicities of the bulges are on average twice lower in the isolated S0s compared to all of the other samples. We can speculate that this difference may be related to the possible difference in gas accretion sources in S0 galaxies in different environments, if the SSP-equivalent metallicity of the bulges is biased toward the metallicity of the last stellar generation born during some bulge rejuvenation event.

5.2. Rings and Lenses

The general structure of lenticular galaxies differs from that of other disk galaxies by often revealing such disk features as stellar rings (most frequent in S0/a, de Lapparent et al. 2011) and lenses (most frequent in S0s, Laurikainen et al. 2009). It is a common view that the stellar lenses are very old and dynamically hot, although this point of view is based on very rare observations of a few objects (Kormendy 1984; Laurikainen et al. 2013). We have succeeded in measuring kinematical and stellar population characteristics for nine lenses and rings, and our results contradict this common view. The stellar velocity dispersions are generally the same in the lenses or rings and in the surrounding disks (Figure 9, right bottom plot), so dynamically they are indistinguishable; perhaps there are some hints that the rings and lenses can be found mostly in dynamically hot disks. Figure 9 also gives evidence for the identical chemical properties of the lenses or rings and their surrounding disks. But there is one important distinction between the disks and the lenses or rings: while the mean stellar ages of the disks fill out the complete range of

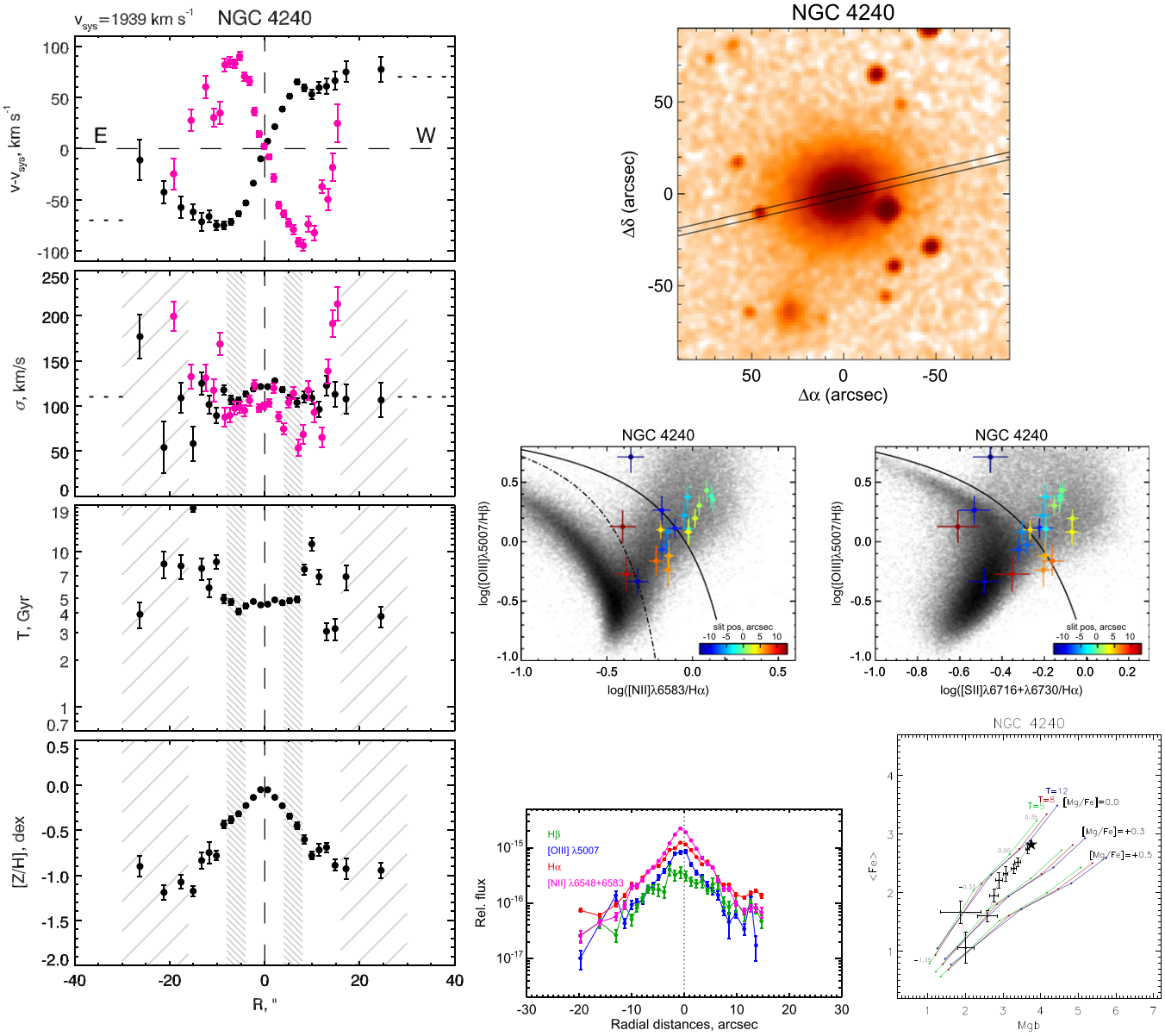

Figure 16. NGC 4240. The same as the previous figure.

possible values, between 1 and 12 Gyr, the ages of the rings and lenses are predominantly concentrated in the narrow range between 2 and 6 Gyr (Figure 9, left upper plot). An exception is the galaxy from the SCORPIO sample, NGC 6615, which has the largest ring among the entire sample, with the age of ≈13 Gyr. We can thus state that the last star-forming episodes took place in these substructures at $z < 1$. Here we see an association with the fact that strong bars are predicted to appear in galactic disks only after $z = 1$ (Kraljic et al. 2012). Because lenses in S0s are commonly related to dissolved or weakened bars (Buta et al. 2010), and because star formation in rings is usual at the resonance radii of the bars (Buta & Combes 1996), we would like to connect the epoch of the last star-forming episodes in the rings and lenses and the epoch of the rapid bar arising in the stellar disks after $z < 1$.

Another interesting finding can be seen in Figure 10. Whereas the bulges show the correlation between their ages and the stellar velocity dispersion, just as is known for elliptical galaxies, the ages of disks and rings or lenses do not correlate with the observed stellar velocity dispersion. These findings are supported by the evaluation of the Spearman correlation coefficient between the ages and the velocity dispersion of the bulges, $r_s = 0.58$, with the probability of the correlation an insignificant $p = 0.012$, whereas the correlation coefficients for the disks, $r_s = 0.07$, $p = 0.80$, and for the rings or lenses, $r_s = -0.17$, $p = 0.61$, prove that here the dependencies are absent. In addition, we found a slight anticorrelation between the stellar metallicity and velocity dispersion in the ring or lens structures ($r_s = -0.46$, $p = 0.15$), whereas for the disks and bulges the correlation is insignificant ($r_s = -0.26$, $p = 0.34$ for the disks and $r_s = 0.12$, $p = 0.62$ for the bulges). It is obvious that such an anticorrelation, if it exists, has an evolutionary census, but an extension of the galaxy sample with reliable measurements of the stellar population properties in the disk substructures is needed to strengthen the relation and to propose a particular scenario to explain it.

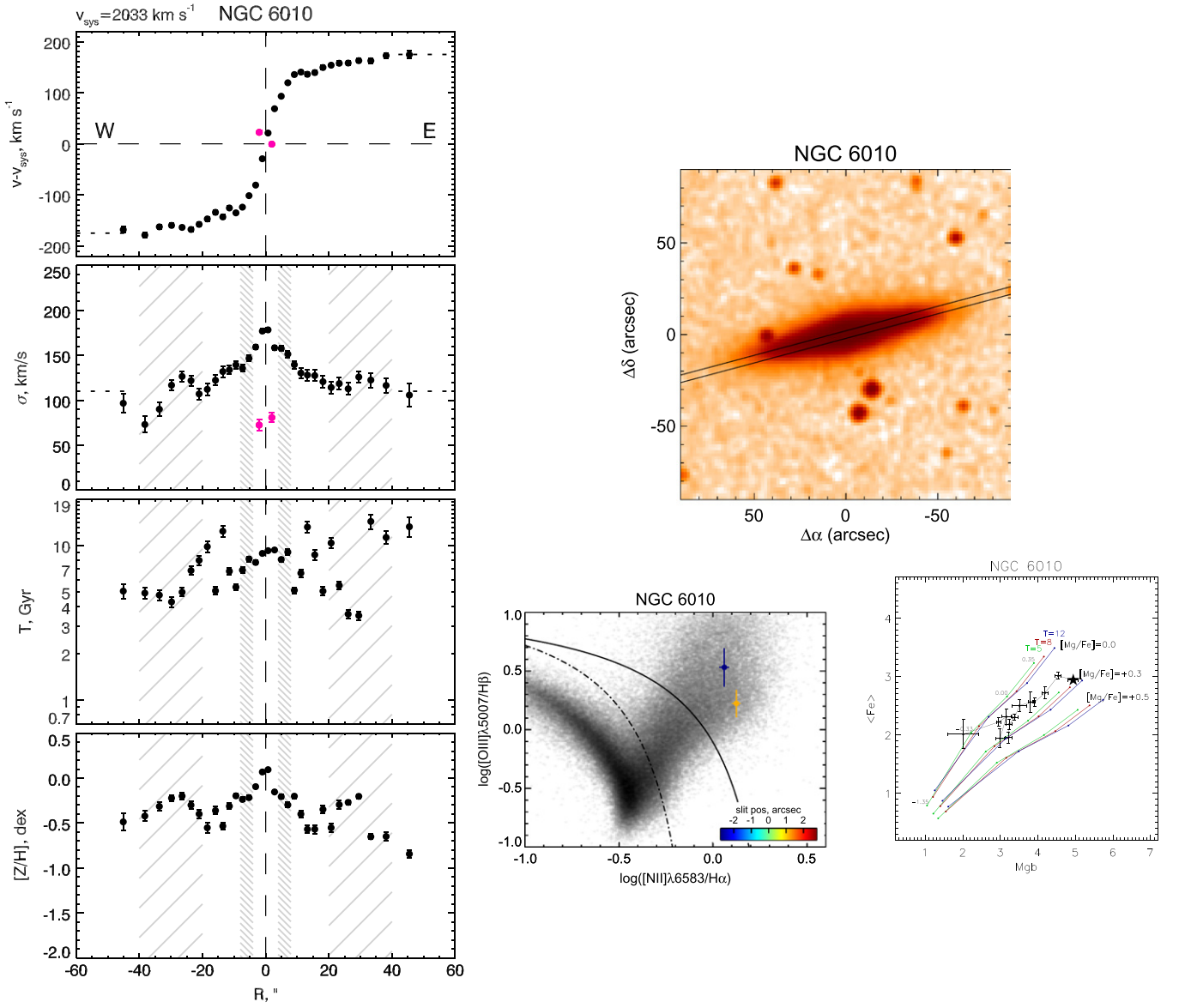

Figure 17. NGC 6010. The same as the previous figure.

5.3. Ionized-gas Characteristics

By analyzing the half of our sample observed at the Russian 6 m telescope, we have noted that, first, the majority of isolated lenticular galaxies contain extended ionized-gas disks, and second, the rotation and orientation of the ionized-gas disks are often decoupled from the rotation and orientation of the stellar disks (Katkov et al. 2014a). Now, with the complete sample in hand, we can refine the statistics of the ionized-gas content of the isolated lenticular galaxies. Among the 18 galaxies studied, 13 galaxies demonstrate extended ionized-gas emission ($72\% \pm 11\%$); among the 13 galaxies with the extended gas emission, seven galaxies ($54\% \pm 14\%$) demonstrate visible counterrotation of the ionized gas with respect to their stellar components. Our spectral observations are "one-dimensional": the long slit aligned with the major axis of the continuum isophotes characterizing the line of nodes of the *stellar* disk cannot help to determine the orientation of the *gas* rotation plane. Following the logic proposed by Bertola et al. (1992), if we suppose that the gas in S0s is accreted from external sources, and the orbital momentum of the accreted gas is oriented accidentally with respect to the angular momentum of the galaxy, we should see equal proportions of corotating and counterrotating gas by studying only the gas velocity projection onto the stellar disk lines of nodes. This is just what we have found from our observations of the isolated lenticular galaxies, so we may conclude that the statistics of the ionized-gas rotation in our sample of the isolated lenticular galaxies gives evidence for *all* of the gas having been accreted from external sources isotropically distributed around the galaxies.

What can these sources be? Because our galaxies are *isolated* and do not have neighboring large galaxies that may be donors of the gas, we can propose only two probable sources for the decoupled gas acquisition: minor merging of small gas-rich satellites (Reshetnikov & Sotnikova 1997; Bournaud & Combes 2003) or gas inflow from cosmological filaments of the universe's large-scale structure (Kereš et al. 2005; Dekel & Birnboim 2006; Bournaud & Elmegreen 2009). We suggest that the metallicity of the gas can help to identify exactly the origin of the gas: cosmological filaments of the universe's

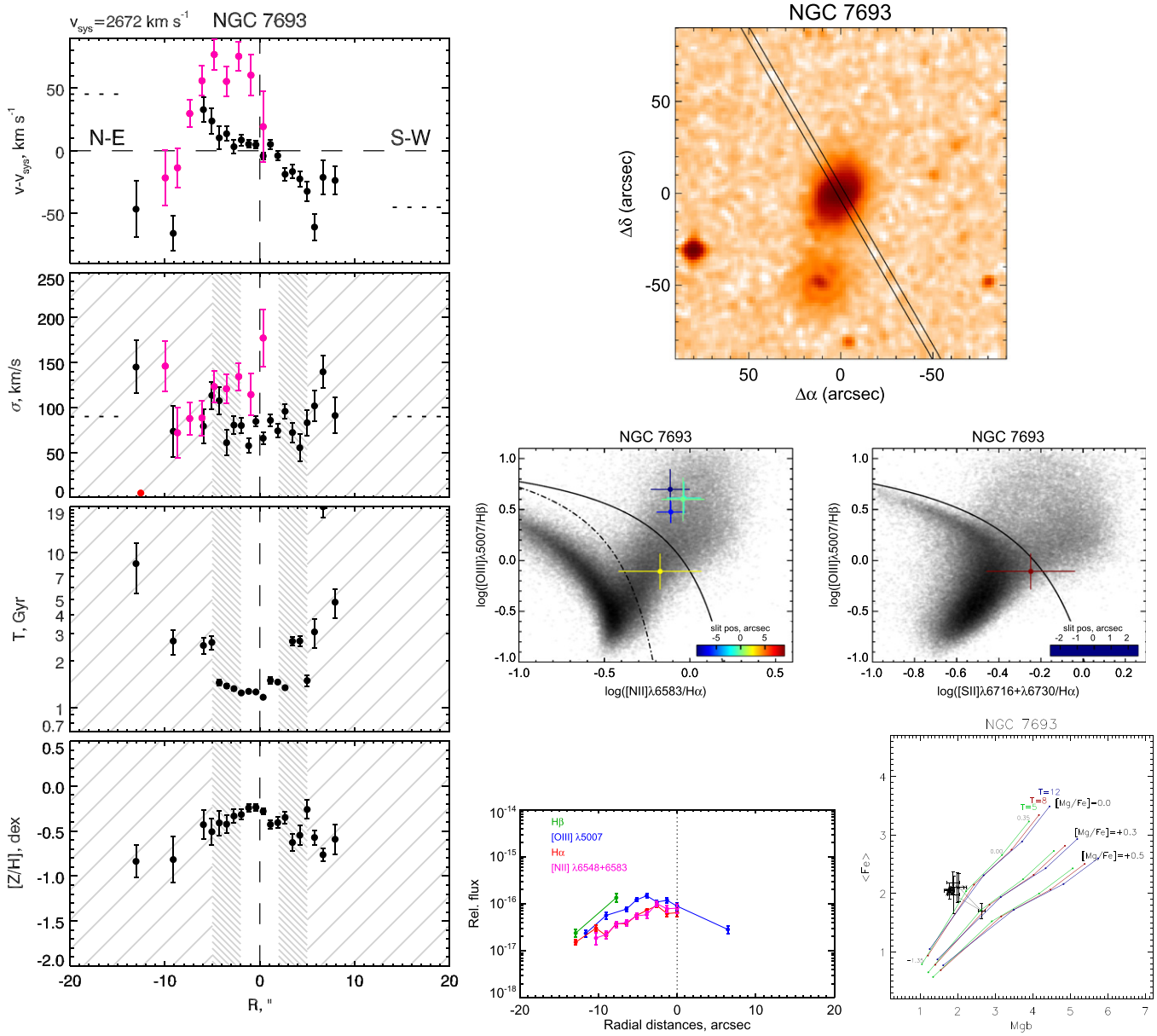

Figure 18. NGC 7693. The same as the previous figure.

large-scale structure must contain pristine gas, so it must be very metal-poor (Agertz et al. 2009). By pursuing this aim, we have picked out in our galaxies the radial ranges along the slit where the ionized gas is excited by young stars, according to the BPT-diagram diagnostics, and then we have added the spectra over these ranges for every galaxy. To these rather high-S/N spectra, we have applied so-called "strong-line calibrations," allowing us to estimate the oxygen abundance in the H II regions with only a few emission lines, namely, with the Balmer lines Hα and Hβ, low-excitation [N II]λ6583, and high-excitation [O III]λ5007. We have succeeded in estimating the metallicity of the ionized gas in eight isolated lenticular galaxies. The results are presented in the Table 3. Despite the wide range of galaxy luminosities, the ionized-gas metallicities appear to be confined to a very narrow range of values near the solar metallicity or slightly higher. Therefore, we think that we can exclude cosmological filaments as the source of gas accretion in this particular case. Obviously, we see the consequences of gas-rich satellite merging.

Though formally we cannot determine the orientation of the ionized-gas rotation plane with only long-slit spectroscopy, we can note some possible signatures of gas confinement to the plane of the stellar disk: it may be the consistency of the rotation velocity estimates for the stars and for the gas in the outer parts of the galaxies where the stellar velocity dispersion is low and does not affect strongly the line-of-sight velocity profiles through the asymmetric drift. Within our sample, such consistency is demonstrated by the galaxies with corotating ionized gas IC 1608, NGC 1211, NGC 2350, NGC 2917, and UGC 9980, and by the galaxies with *counterrotating* ionized gas NGC 4240 and NGC 6798; just these galaxies figure in Table 3 with their outer ionized gas excited by young stars. Other galaxies, where we can suspect the gas is rotating off the main symmetry plane, show mostly other types of excitation—by shock waves or by old post-asymptotic giant

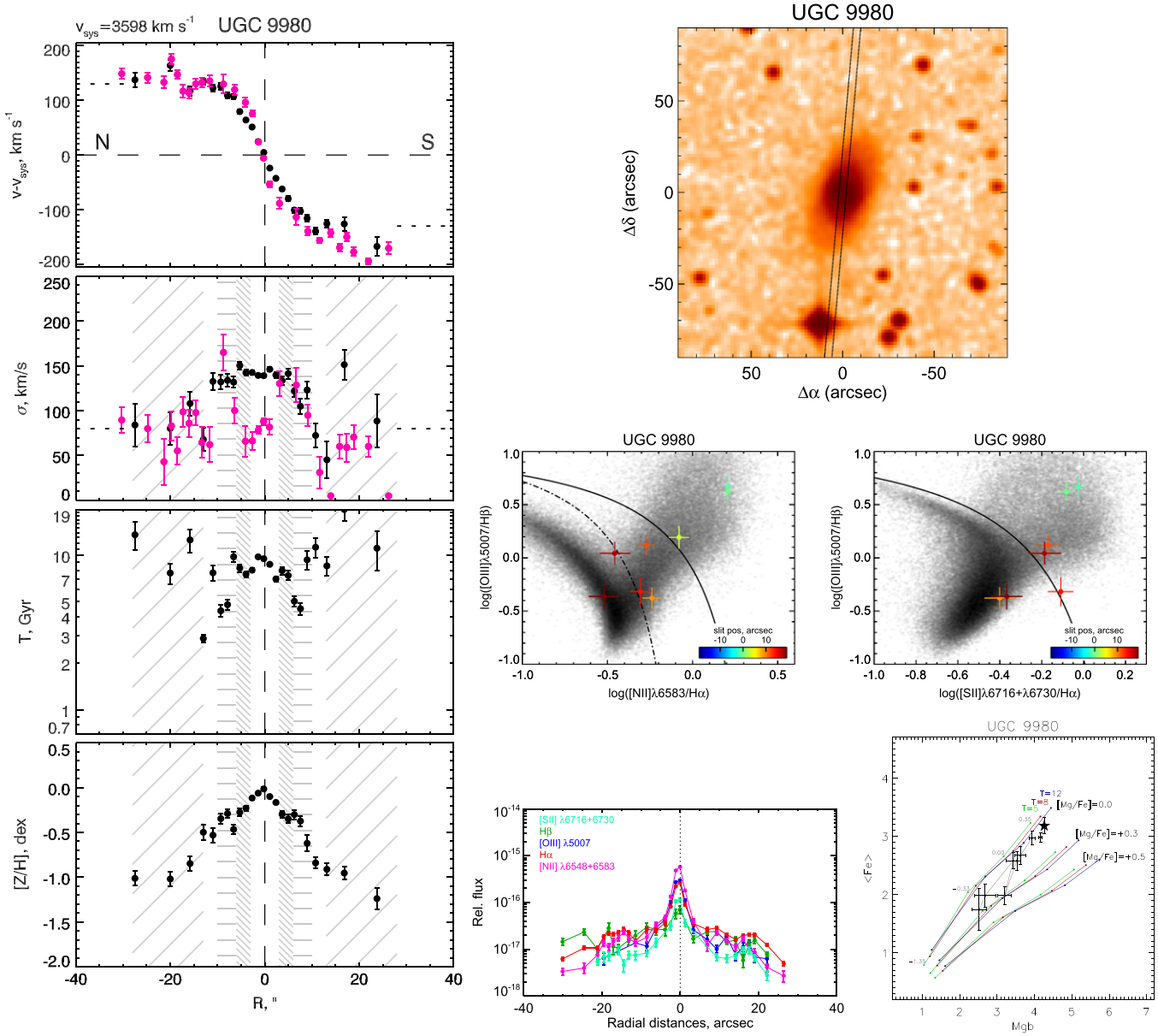

Figure 19. UGC 9980. The same as the previous figure.

branch (AGB) stars—placing the emission-line flux ratios in the BPT diagrams to the right of the dividing curve. We can here remember the theoretical consideration by Wakamatsu (1993), who noted that inclined gaseous disks or rings must experience shocks developed by the gas crossing the gravitational potential well of a stellar disk. The shock waves must heat the gas and prevent its cooling necessary for a star-formation burst. We suggest then that the conditions for star formation starting in the accreted gas must also include, besides the gas amount, the favorable geometry of the gas accretion.

5.4. Origin of Isolated S0s

At this point we would like to start a discussion about the origin of isolated lenticular galaxies. Indeed, all of the mechanisms proposed so far to quench star formation in the disks of spiral galaxies and to transform them into lenticulars act only in dense environments—in clusters and massive rich groups. It thus remained quite unclear how lenticular galaxies in the field might form. The situation changes if we accept the new paradigm for the evolution of disk galaxies proposed by Sil'chenko et al. (2012): all disk galaxies started their evolution as lenticulars at the redshifts of $z = 2$–3, and only after $z < 1$ most of them became spirals by undergoing persistent outer gas accretion onto their disks, which resulted in dynamical cooling and subsequent spiral-arm development and star-formation ignition. Then the key point for galaxy morphological shaping becomes the outer-gas accretion regime. In clusters, the outer cold gas accretion is almost impossible due to tide-induced starvation and hot intracluster medium ram pressure, so in clusters most disk galaxies remain as lenticulars for all of their lives. In the field, the conditions for outer cold gas accretion can be quite varied. If we regard gas-rich satellite merging as a main outer gas source, then we can expect the following variety of satellite system properties for the isolated disk galaxies: How many satellites does the host galaxy have? Are they distributed

Table 3
Estimates of the Ionized-gas Oxygen Abundance in the Emission Regions Excited by Young Stars

Galaxy	Radial Range of Binning, (arcseconds)	12+log O/H ($[Z/H]_O$), (dex)
	SALT data	
IC 1608	(−51.4; −31.1)	8.78 (0.09) ± 0.47
	(29.7; 43.4)	8.80 (0.11) ± 0.26
NGC 1211 ^{N2}	(9.4; 15.8)	8.72 (0.03) ± 0.41
	(32.3; 37.3)	8.73 (0.04) ± 0.41
NGC 2917	(−15.7; −5.6)	8.90 (0.21) ± 0.27
	(9.6; 19.8)	8.82 (0.13) ± 0.26
NGC 4240 ^{N2}	(−11.6; −6.6)	8.80 (0.11) ± 0.41
	(4.1; 12.2)	8.78 (0.09) ± 0.41
UGC 9980 ^{N2}	(−13.1; −4.3)	8.82 (0.13) ± 0.42
	(8.4; 20.8)	8.71 (0.02) ± 0.42
	SCORPIO data	
NGC 2350	(−1.6; 2.0)	8.68 (−0.01) ± 0.25
NGC 6798 ^{N2}	(−34.1; −27.7)	8.71 (0.02) ± 0.41
	(29.1; 36.6)	8.73 (0.04) ± 0.41
NGC 7351	(−2.7; 3.8)	8.64 (−0.05) ± 0.25

Note. N2 marks the estimations that were done by using only the N2 emission line index.

isotropically around it, or are they confined to some dedicated plane, as is observed in our Galaxy and in M31? Is the satellite system dynamically cold or hot (related perhaps to the mass of the host dark matter halo)? Concerning the last point, there is a curious fact noticed by Karachentseva et al. (2011). They considered faint companions of isolated galaxies from their catalog 2MIG. They found that the companions of isolated *early-type* galaxies have on average a larger line-of-sight velocity difference from their hosts than for the late-type ones. By inspecting their Figure 4, we have ascertained that there are no practically companions of isolated early-type galaxies with a line-of-sight velocity difference less than 50 km s^{-1}, whereas the isolated late-type hosts possess many such companions. It is a natural suggestion that the accretion of companions with a large flyby velocity is more difficult than that of slow ones, so we come to the conclusion that perhaps just a "hot" orbital population of companions defines an early morphological type of the host isolated galaxy. Perhaps the orbital composition of a satellite system is related stochastically to the initial conditions, or maybe a present-day isolated lenticular merged all of its slow companions several gigayears ago and has none presently. In other cases, the accretion of a gas-rich satellite from a highly inclined orbit may lead to gas heating and prevent star formation and spiral-arm development, which requires a cold, gravitationally unstable disk. By trying possible variants of the satellite merging regime, we can easily get an isolated galaxy of any morphological type—in comparison to the tight accretion conditions in dense environments, which provide a subsequent tight range of morphological types, mostly S0s.

6. SUMMARY

We have observed nine galaxies from our sample of isolated lenticular galaxies at the 10 m SALT with the RSS in the long-slit mode. The radial variations of the kinematical characteristics, line-of-sight velocities, and velocity dispersions are studied both for the stellar component and for the ionized gas that is found in the largest part of the sample. We have also derived radial profiles of the mean stellar metallicity and ages, as well as the gas excitation characteristics and oxygen abundances far outward into the disk-dominated regions of the galaxies. By joining the two subsamples of isolated lenticular galaxies studied by us here and earlier, the northern and southern ones, with a total of 18 isolated lenticular galaxies, we analyze the statistics of the stellar population properties and ionized-gas features for this morphological type of galaxies in extremely rarefied environments.

We have found that there is no particular time frame for shaping the isolated lenticular galaxies: the mean stellar ages of the bulges and disks are homogeneously distributed between 1 and >13 Gyr, and the bulges and disks tend to form synchronously, having mostly similar ages and magnesium-to-iron ratios. In some galaxies, we found stellar disk substructures, rings and lenses, and their mean stellar ages are confined to a rather narrow range, from 2 to 5 Gyr. We relate the appearance of these structures to the strong bars arising in disk galaxies after $z < 1$.

An ionized-gas extended emission is found in the majority of our galaxies, in 13 of 18 ($72\% \pm 11\%$), and half of all extended gaseous disks visibly demonstrate a counterrotation with respect to their stellar counterparts. Just such a proportion is expected if all of the gas in isolated lenticular galaxies is accreted from isotropically distributed external sources. A very narrow range of oxygen abundances, [O/H] from 0.0 to +0.2 dex, estimated by us for the outer ionized-gas disks excited by young stars, gives evidence for satellite merging as the most probable source of this accretion. Finally, we formulate a hypothesis that the morphological type of a field disk galaxy is completely determined by the outer cold gas accretion regime.

The observations reported in this paper were obtained with the Southern African Large Telescope (SALT). A.Y.K. acknowledges the support from the National Research Foundation (NRF) of South Africa. The study of isolated lenticular galaxies is supported by grant No. 13-02-00059a of the Russian Foundation for Basic Research. I.Y.K. is grateful to Dmitry Zimin's nonprofit Dynasty Foundation.

Funding for SDSS-III has been provided by the Alfred P. Sloan Foundation, the Participating institutions, the National Science Foundation, and the U.S. Department of Energy Office of Science. The SDSS-III web site is http://www.sdss3.org/. SDSS-III is managed by the Astrophysical Research Consortium for the participating institutions of the SDSS-III Collaboration, including the University of Arizona, the Brazilian Participation Group, Brookhaven National Laboratory, Carnegie Mellon University, University of Florida, the French Participation Group, the German Participation Group, Harvard University, the Instituto de Astrofisica de Canarias, the Michigan State/Notre Dame/JINA Participation Group, Johns Hopkins University, Lawrence Berkeley National Laboratory, Max Planck Institute for Astrophysics, Max Planck Institute for Extraterrestrial Physics, New Mexico State University, New York University, Ohio State University, Pennsylvania State

University, University of Portsmouth, Princeton University, the Spanish Participation Group, University of Tokyo, University of Utah, Vanderbilt University, University of Virginia, University of Washington, and Yale University.

REFERENCES

Agertz, O., Teyssier, R., & Moore, B. 2009, MNRAS, 397, L64
Baldwin, J. A., Phillips, M. M., & Terlevich, R. 1981, PASP, 93, 5
Bertola, F., Buson, L. M., & Zeilinger, W. W. 1992, ApJL, 401, L79
Binney, J. 1978a, ComAp, 8, 27
Binney, J. 1978b, MNRAS, 183, 501
Birnboim, Y., Dekel, A., & Neistein, E. 2007, MNRAS, 380, 339
Bournaud, F., & Combes, F. 2003, A&A, 401, 817
Bournaud, F., & Elmegreen, B. G. 2009, ApJL, 694, L158
Buckley, D. A. H., Swart, G. P., & Meiring, J. G. 2006, Proc. SPIE, 6267, OZ
Burgh, E. B., Nordsieck, K. H., Kobulnicky, H. A., et al. 2003, Proc. SPIE, 4841, 1463
Buta, R., & Combes, F. 1996, FCPh, 17, 95
Buta, R., Laurikainen, E., Salo, H., et al. 2010, ApJ, 721, 259
Byrd, G., & Valtonen, M. 1990, ApJ, 350, 89
Cappellari, M., & Emsellem, E. 2004, PASP, 116, 138
Cappellari, M., Emsellem, E., Krajnović, D., et al. 2011, MNRAS, 416, 1680
Chilingarian, I., Prugniel, P., Sil'Chenko, O., et al. 2007a, in IAU Symp. 241, Stellar Populations as Building Blocks of Galaxies, ed. A. Vazdekis & R. Peletier (Cambridge: Cambridge Univ. Press), 175
Chilingarian, I. V. 2009, MNRAS, 394, 1229
Chilingarian, I. V., Prugniel, P., Sil'Chenko, O. K., et al. 2007b, MNRAS, 376, 1033
Cid Fernandes, R., Mateus, A., Sodré, L., et al. 2005, MNRAS, 358, 363
Crawford, S. M., Still, M., Schellart, P., et al. 2010, Proc. SPIE, 7737, 25
Davis, T. A., Alatalo, K., Sarzi, M., et al. 2011, MNRAS, 417, 882
de Lapparent, V., Baillard, A., & Bertin, E. 2011, A&A, 532, A75
Dekel, A., & Birnboim, Y. 2006, MNRAS, 368, 2
Dressler, A. 1980, ApJ, 236, 351
Faber, S. M., Friel, E. D., Burstein, D., et al. 1985, ApJS, 57, 711
Garcia-Appadoo, D. A., West, A. A., Dalcanton, J. J., et al. 2009, MNRAS, 394, 340
Gunn, J. E., & Gott, J. R., III 1972, ApJ, 176, 1
Hau, G. K. T., & Forbes, D. A. 2006, MNRAS, 371, 633
Howell, J. H. 2005, AJ, 130, 2065
Hubble, E. P. 1936, Realm of the Nebulae (New Haven: Yale Univ. Press)
Icke, V. 1985, A&A, 144, 115
Illingworth, G. 1977, ApJL, 218, L43
Johnston, E. J., Aragón-Salamanca, A., & Merrifield, M. R. 2014, MNRAS, 441, 333
Karachentsev, I. D., Karachentseva, V. E., Huchtmeier, W. K., et al. 2004, AJ, 127, 2031
Karachentsev, I. D., & Makarov, D. I. 2008, AstBu, 63, 299
Karachentsev, I. D., Makarov, D. I., & Kaisina, E. I. 2013, AJ, 145, 101
Karachentsev, I. D., Makarov, D. I., Karachentseva, V. E., et al. 2011, AstBu, 66, 1
Karachentseva, V. E., Karachentsev, I. D., & Melnyk, O. V. 2011, AstBu, 66, 389
Katkov, I. Y., Sil'chenko, O. K., & Afanasiev, V. L. 2014a, MNRAS, 438, 2798
Katkov, I. Y., Silchenko, O. K., & Afanasiev, V. L. 2014b, AstBu, 69, 121
Kauffmann, G., Heckman, T. M., Tremonti, C., et al. 2003, MNRAS, 346, 1055
Kereš, D., Katz, N., Weinberg, D. H., et al. 2005, MNRAS, 363, 2
Kewley, L. J., Groves, B., Kauffmann, G., et al. 2006, MNRAS, 372, 961
Kniazev, A. Y., Zijlstra, A. A., Grebel, E. K., et al. 2008, MNRAS, 388, 1667
Kobulnicky, H. A., Nordsieck, K. H., Burgh, E. B., et al. 2003, Proc. SPIE, 4841, 1634
Kormendy, J. 1984, ApJ, 286, 116
Kormendy, J. 1993, in IAU Symposium. 153, Galactic Bulges, ed. H. Dejonghe & H. J. Habing (Dordrecht: Kluwer), 209
Kormendy, J., & Bender, R. 2012, ApJS, 198, 2
Kormendy, J., & Kennicutt, R. C., Jr. 2004, ARA&A, 42, 603
Kraljic, K., Bournaud, F., & Martig, M. 2012, ApJ, 757, 60
Larson, R. B., Tinsley, B. M., & Caldwell, C. N. 1980, ApJ, 237, 692
Laurikainen, E., Salo, H., Athanassoula, E., et al. 2013, MNRAS, 430, 3489
Laurikainen, E., Salo, H., Buta, R., et al. 2009, ApJL, 692, L34
Laurikainen, E., Salo, H., Buta, R., et al. 2010, MNRAS, 405, 1089
le Borgne, D., Rocca-Volmerange, B., Prugniel, P., et al. 2004, A&A, 425, 881
Makarov, D., & Karachentsev, I. 2011, MNRAS, 412, 2498
Makarov, D. I., & Karachentsev, I. D. 2009, AstBu, 64, 24
Mitronova, S. N., Karachentsev, I. D., Karachentseva, V. E., et al. 2004, BSAO, 57, 5
Moore, B., Katz, N., Lake, G., et al. 1996, Natur, 379, 613
Naim, A., Lahav, O., Buta, R. J., et al. 1995, MNRAS, 274, 1107
Nelan, J. E., Smith, R. J., Hudson, M. J., et al. 2005, ApJ, 632, 137
Ocvirk, P., Pichon, C., Lançon, A., et al. 2006, MNRAS, 365, 74
O'Donoghue, D., Buckley, D. A. H., Balona, L. A., et al. 2006, MNRAS, 372, 151
Pettini, M., & Pagel, B. E. J. 2004, MNRAS, 348, L59
Prugniel, P., Soubiran, C., Koleva, M., et al. 2007, arXiv:astro-ph/0703658
Quilis, V., Moore, B., & Bower, R. 2000, Sci, 288, 1617
Reda, F. M., Proctor, R. N., Forbes, D. A., et al. 2007, MNRAS, 377, 1772
Reshetnikov, V., & Sotnikova, N. 1997, A&A, 325, 933
Richter, O.-G., & Huchtmeier, W. K. 1987, A&AS, 68, 427
Salpeter, E. E. 1955, ApJ, 121, 161
Sancisi, R., Fraternali, F., Oosterloo, T., et al. 2008, A&ARv, 15, 189
Shaya, E. J., & Tully, R. B. 1984, ApJ, 281, 56
Sil'chenko, O. K. 2006, ApJ, 641, 229
Sil'chenko, O. K. 2008, in IAU Symp. 245, Formation and Evolution of Galaxy Bulges, ed. M. Bureau, E. Athanassoula & B. Barbuy (Cambridge: Cambridge Univ. Press), 277
Sil'Chenko, O. K., Chilingarian, I. V., Sotnikova, N. Y., et al. 2011, MNRAS, 414, 3645
Sil'chenko, O. K., Kniazev, A. Y., & Chydakova, E. M. 2015, AstBu, in press
Sil'chenko, O. K., Proshina, I. S., Shulga, A. P., et al. 2012, MNRAS, 427, 790
Spitzer, L., Jr., & Baade, W. 1951, ApJ, 113, 413
Springob, C. M., Haynes, M. P., Giovanelli, R., et al. 2005, ApJS, 160, 149
Sulentic, J. W., Verdes-Montenegro, L., Bergond, G., et al. 2006, A&A, 449, 937
Thomas, D., Maraston, C., & Bender, R. 2003, MNRAS, 339, 897
Thomas, D., Maraston, C., Bender, R., et al. 2005, ApJ, 621, 673
Trager, S. C., Faber, S. M., Worthey, G., et al. 2000, AJ, 120, 165
van den Bergh, S. 1976, ApJ, 206, 883
van der Marel, R. P., & Franx, M. 1993, ApJ, 407, 525
Wakamatsu, K.-I. 1993, AJ, 105, 1745
Worthey, G., Faber, S. M., Gonzalez, J. J., et al. 1994, ApJS, 94, 687
Worthey, G., & Ottaviani, D. L. 1997, ApJS, 111, 377